ACS APPLIED MATERIALS & INTERFACES

www.acsami.org

Research Article

Simultaneous Light-Triggered Release of Nitric Oxide and Carbon Monoxide from a Lipid-Coated Upconversion Nanosystem Inhibits Colon Tumor Growth

Yaw Opoku-Damoah, Run Zhang,* Hang T. Ta, and Zhi Ping Xu*

Cite This: *ACS Appl. Mater. Interfaces* 2023, 15, 56796−56806

Read Online

ACCESS | Metrics & More | Article Recommendations | Supporting Information

ABSTRACT: Gas therapy has gained noteworthy attention in biomedical research, with the rise of gas-releasing molecules enhancing their therapeutic potential, especially when integrated into nano-based drug delivery systems. Herein, we present a lipid-coated gas delivery system to simultaneously shuttle two gas-releasing molecules carrying nitric oxide (NO) and carbon monoxide (CO), respectively. Upconversion nanoparticles (UCNPs) are designed to generate photons at 360 nm upon 808 nm of near-infrared (NIR) irradiation. These in situ-generated UV photons trigger simultaneous NO and CO release from *S*-nitrosoglutathione (GSNO) and the CO-releasing molecule (CORM), respectively, which are coloaded into lipid-coated UCNP/GSNO/CORM/FA nanoparticles (LUGCF). LUGCF with a GSNO/CORM mass ratio of 2:1 is determined to be optimal in terms of synergistically instigating apoptosis in HCT116 and CT26 colon cancer cells, where both NO/CO are released and subsequent production of ROS are detected. This CO/NO combination nanoplatform exhibits a very effective inhibition of colon tumor growth in vivo at relatively low doses upon a mild 808 nm irradiation. Overall, we effectively integrated two therapeutic gas-releasing molecules in one NIR-responsive nanosystem, presenting a promising therapeutic strategy for future biomedical applications in dual-gas cancer therapy.

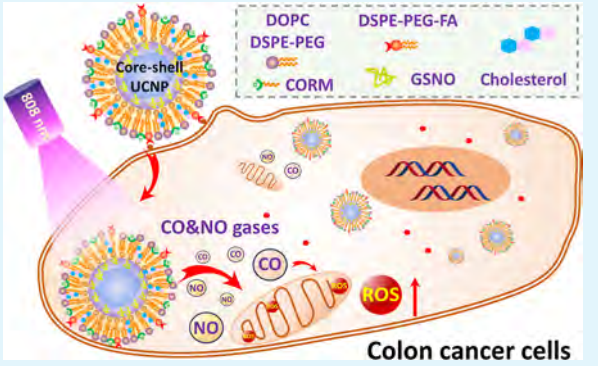

KEYWORDS: *carbon monoxide, nitric oxide, light-triggered gas delivery, upconversion nanoparticle, colon cancer treatment*

1. INTRODUCTION

Nanotechnology has revolutionized drug delivery and controlled drug release for the treatment of different kinds of diseases. In recent years, various nanomedicines have been synthesized with liquid and solid active ingredients and explored for effective cancer therapy. Their size, biocompatibility, responsive release, and site-specific targeting ability have paved the way for advanced laboratory and clinical development.[1] On the other hand, nano-based gas therapy is gradually gaining attention because of the intrinsic pre-existence and effective roles in different biological systems.[2] Unlike liquid and solid active ingredients, gas molecules are more difficult to formulate into the nanosystem and deliver to the specific site. Alternatively, gases such as carbon monoxide (CO), nitric oxide (NO), sulfur dioxide (SO_2), and hydrogen sulfide (H_2S) are conjugated to various molecules to facilitate their formulation, delivery, and release specifically by internal and/or external stimuli.[2−4] This technique fits well into the multiapproach schemes for multifaceted nano-inspired combination cancer therapy.

The therapeutic effects of these gases have been largely traced back to their biological roles as gasotransmitters in the body.[5] It has been reported that they have potential to cure diseases including cancer, inflammation, and cardiovascular diseases.[6] NO's internal production is mediated by NO synthase, a common enzyme found in tissues in the presence of L-arginine, oxygen, and nicotinamide adenine dinucleotide phosphate.[3] Higher concentrations of NO produce reactive nitrogen species (RNS), similar to reactive oxygen species (ROS), resulting in DNA base deamination and impairing cellular function and enzyme nitrosylation.[7−9] Apart from physiologically regulating cGMP,[10] NO also facilitates the dilation of blood vessels around tumors, thereby enhancing accumulation of drugs and particulates.[11,12] Therefore, NO has been used to enhance or sensitize various chemotherapy of cancer drugs and we seek to employ this strategy to codeliver it with CO gas to enhance CO molecule accumulation.[13,14] Similarly, CO is synthesized internally via the enzymatic

Received: September 3, 2023
Revised: November 16, 2023
Accepted: November 16, 2023
Published: December 1, 2023

Scheme 1. Schematic Illustration of Synthesis Procedure Involving OA Removal from UCNPs and Conjugation of DOPA Lipid and GSNO Followed by Co-encapsulation of CORM into Lipid Bilayers[a]

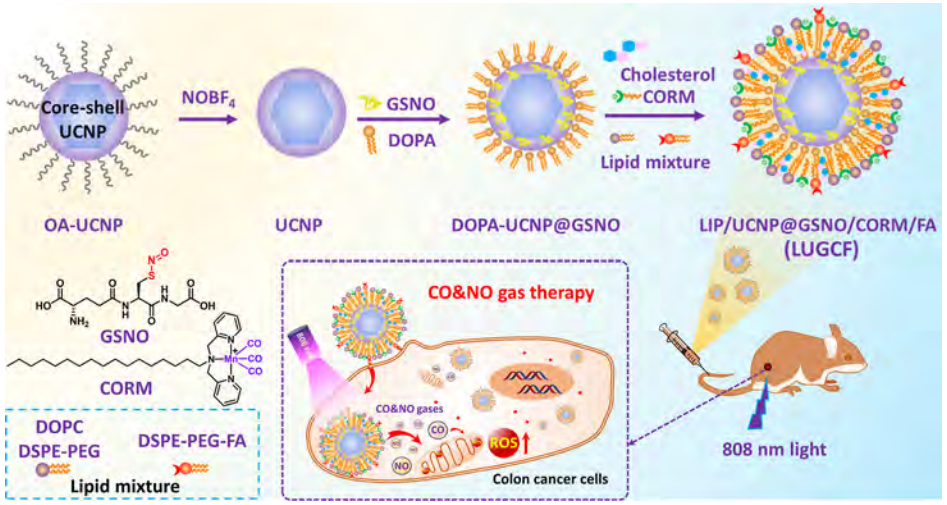

[a]The final LUGCF nanoparticles are taken up by cancer cells and both CO and NO gases are responsively released in situ by conversion of 808 nm light to 360 nm photons.

activity of heme oxygenase that degrades heme.[15] CO produces a characteristic anti-Warburg effect by stimulating bioenergetics in cancer cells, which may result in rapid metabolic exhaustion. CO also targets the mitochondria in tumor cells, consuming a high level of oxygen and triggering the generation of ROS to cause the mitochondrial collapse.[16−18] It is also evident that these two gasotransmitters share common signaling pathways and similar regulatory functions.[19]

Therefore, gas-releasing molecules have been the main driving force toward achieving a suitable gas therapy of various diseases,[20] and the successful caging of therapeutic gases within nanoplatforms is essential for their delivery.[3,11] The strategy basically involves molecules that can easily load gases for a responsive release. For example, a series of metal carbonyls that can release CO under internal conditions such as low pH,[21,22] ROS,[23,24] biomolecules,[25] and/or with the application of external stimulus, such as light,[26,27] ultrasound,[28] and magnetic field.[29] Similarly, most stimulus-responsive NO-releasing molecules (NORMs) are naturally occurring compounds or organic compounds modified with specific groups that have the capacity to release NO upon stimulation.[30,31] These include *S*-nitrosothiols,[32,33] *N*-diazeniumdiolate (NONOate),[34,35] *N*-nitrosoamines,[36,37] organic nitrates, and alkyl substituted nitrobenzenes.[38,39] These gas-releasing molecules require protection in the biological system, and nanocarriers offer the ability to shuttle, protect, and moderate their release at the target site.

Light-responsive platforms have proven to be the most effective for nano-based gas release systems due to the efficient response in penetrating tissues, cleaving bonds, and producing heat for release with their noninvasive and biofriendly nature.[40] However, most of the gases are covalently bound to releasing molecules and require UV light to trigger, which has less penetration depths.[41−43] Li et al. produced an NIR-responsive $Fe(CO)_5$ PEG-NH_2 delivery system employing mesoporous Prussian blue nanoparticles as the photothermal agent to elevate the temperature after irradiation for cancer therapy.[44] In another study, Garcia et al. also developed $NaYF_4$:Yb, Er UCNPs capped with mesoporous silica nanoshell for NO release from Roussin's black salt.[45] They employed 980 nm light to produce photons in the visible region to trigger a NO release. The risk of overheating, limited penetration, and water absorption associated with a 980 nm light may reduce the efficacy of such systems and therefore the less invasive 808 nm is required for advanced studies.[46−48] Moreover, there is no report regarding a NIR-responsive delivery system for simultaneous dual release of two gases (such as NO and CO) for combination cancer gas therapy.

Herein, we report for the first time that an NIR light-responsive lipid delivery system is capable of triggering two gas-releasing molecules (CORM and GSNO, Scheme 1) to simultaneously release two gases. GSNO absorbs UV light at 355 nm (λ_{max}) and the CORM at 365 nm. In this research, simultaneous release of two gasotransmitters (NO and CO) is smartly mediated by core−shell upconversion nanoparticles ($NaYF_4$, Yb, Tm, Ho@$NaYF_4$, and Nd UCNPs). The UCNPs absorb either 980 or 808 nm NIR light and emit photons in the UV and visible region (360 and 550 nm) that both gas-releasing molecules (CORM and GSNO) absorb efficiently to release NO and CO. As shown in Scheme 1, hydrophilic GSNO renders amphiphilicity after conjugating with 1,2-dioleoyl-*sn*-glycero-3-phosphate (DOPA) to UCNPs via the carboxylic group (−COOH) or phosphate groups (HPO_4^{2-}). CORMs are loaded into the bilayer hydrophobic region as previously reported.[49] These groups cap oleic acid (OA)-free UCNPs via a two-step ligand exchange process to replace the oleate ions on the surface of UCNPs. The constructed nanoparticles (LUGCF) were found to efficiently release both gases in response to NIR laser irradiation for combination therapy of colon cancer (HCT116 and CT26 cells) in vitro and in vivo as this type of cancer has historically demonstrated sensitivity toward gasotransmitters.

2. EXPERIMENTAL SECTION

2.1. Synthesis of Lipid Nanoformulations. First, DOPA-UCNP@GSNO nanoparticles were synthesized and then thin film hydration protocol described previously was used to fabricate lipid nanoparticles.[49,50] In brief, a mixture of 1.1 mg of lipid, containing DOPC, DOPA, cholesterol, DSPE-PEG, and DSPE-PEG-FA with a

https://doi.org/10.1021/acsami.3c13165
ACS Appl. Mater. Interfaces 2023, 15, 56796−56806

lipid molar ratio of 30:10:15:5:5 was added in chloroform (3 mL). DOPA-UCNP@GSNO (containing 1.0 mg of GSNO) and 0.5 mg of CORM were mixed with the above lipid mixture and stirred for 4 h in the dark. The lipid and drug mixture were transferred into a round-bottom flask, and chloroform was removed with a rotary evaporator to obtain a thin film at the bottom of the flask. The flask was left in a desiccator overnight to completely remove any traces of chloroform, followed by slow dissolving of the thin film by 10 mM HEPES buffer of pH = 7.4 at 40 °C. The water-soluble lipid formulation was stirred for 4 h and centrifuged at 20,000*g* for 1 h. The resultant pellet was frozen and lyophilized to determine the final mass before being redissolved in HEPES buffer to obtain the final LUGCF-2:1 (lipid/UCNP/GSNO/CORM/FA) nanoformulation. For LUF (lipid/UCNP/FA) and LUGF (lipid/UCNP/GSNO/FA) nanoformulations, the same procedure was adopted with the addition of only the required drugs or materials. All other nanoformulations with the CORM/GSNO mass ratios of 1:1, 3:1, and 4:1 were prepared by keeping the amount of CORM (0.5 mg) constant and varying the amount of GSNO to optimize the gaseous drug ratios. In addition, LUCF was prepared with DOPA-UCNP without the GSNO conjugation.

2.2. Characterization of Lipid Nanoformulation. The particle morphologies of UCNPs dispersed in cyclohexane and LUGCF nanoformulations in buffer were examined with a Hitachi HT7700A transmission electron microscope. For lipid formulations, 1% phototungsten acid was applied to stain the nanoparticles before transmission electron microscopy (TEM) imaging. The composition features of various nanoparticles prepared at various stages (from the UCNP to final lipid formulation) were determined by Fourier transform infrared (FTIR) spectroscopy. The nanoparticles were completely dried to obtain 1 mg of powder before spectral analysis with a Thermo Scientific Nicolet 6700 FTIR spectrophotometer. Dynamic light scattering was used to measure the surface zeta potential and particle size distribution of all lipid formulations using a Nano-ZS Zetasizer, Malvern Instruments. The colloidal stability of LUGCF-2:1 nanoparticles in HEPES buffer and DMEM was measured at days 2, 4, 6, 8, 10, and 12. UV absorbance spectroscopy (Shimadzu UV−vis 2450 spectrophotometer) was adopted to determine the absorbance of the CORM, GSNO, and lipid nanoformulations in a quartz cuvette. The emission spectra of UCNPs (5 mg/mL) were recorded in a quartz cuvette after irradiation with an external laser (980 and 808 nm) at 1 W/cm^2 in a spectrometer. UCNPs were dispersed in cyclohexane for these spectroscopic tests, and lipid formulations (LUF, LUGF, LUCF, and LUGCF) were detected in HEPES buffer.

2.3. Drug Loading and Loading Efficiency. GSNO loading analysis was performed by CHNS/O elemental analysis (Thermo Scientific FLASH 2000 analyzer). Dry samples of GSNO and lyophilized lipid formulations (1 mg) containing GSNO were used to determine the respective percentages of carbon, hydrogen, and nitrogen. The amount of encapsulated GSNO was determined by calculating the percentages of nitrogen in LUGF and LUGCF-2:1 with respect to the LUF and LUCF samples as controls, respectively. The respective amount of pro-drug CORMs encapsulated in LUCF and LUGCF-2:1 nanoformulations was measured by inductively coupled plasma-optical emission spectroscopy (ICP-OES) analysis of the Mn content using the CORM-free LUF formulation as the control. The capacity for drug loading and the loading efficiency of CORM and GSNO in the nanoformulations were calculated accordingly.

2.4. Spectrophotometric Detection of Gas Release. NIR-light mediated release of CO and NO from LUGCF-2:1 was determined by single or multiple irradiations, with the CO and NO fluorescent probe (COFP and NOFP), respectively.[51,52] First, after laser irradiation (1 W/cm^2), the fluorescence signal of the NO probe was detected at 15 min for the DOPA-UCNP@GSNO intermediary nanoparticle, relative to UV light irradiation. Subsequently, LUGCF-2:1 with CORM (15 μmol) was used for fluorescence measurements. Briefly, COFP (10 μmol) in DMSO was added to the nanoformulation in HEPES buffer, and the fluorescence spectrum (λ_{em} = 520 nm) of the initial mixture in the quartz cuvette was recorded upon excitation at 440 nm using a Shimadzu RF 5301-PC fluorescence spectrophotometer. The mixture was quickly irradiated with a 0.5 W/cm^2 808 nm laser for 5 min and sealed with parafilm throughout the experiment to avoid CO gas escaping. The fluorescence intensity of COFP was recorded at various time intervals.

NO release was determined with a synthesized ruthenium(II) complex NO fluorescent probe (NOFP).[52] LUGCF-2:1 formulation with a GSNO amount of 45 μmol was added to 10 μmol of NO fluorescent probe, and the initial fluorescence intensity (λ_{ex} = 450 nm, λ_{em} = 600 nm) was recorded before irradiation with a 0.5 W/cm^2 808 nm laser for 5 min. The cuvette was quickly sealed and the fluorescence intensity of the mixture at predetermined intervals recorded. The unreleased amounts of CO and NO were determined by irradiating the mixture at 2 h after the initial irradiation, and the intraday fluorescence intensity for both CO probe and NO probe were subsequently determined for 7 consecutive days.

2.5. Intracellular Gas Release (NO and CO). HCT116 cells (2 × 10^4) were seeded in 12-well plates with coverslips at the bottom. After 24 h of incubation, intracellular CO was detected by incubating the cells with fresh media containing LUGCF-2:1 (15 μmol of CORM). Before replacement with fresh media containing 10 μmol of COFP, the cells were incubated at 37 °C for 4 h, followed by irradiation with an 808 nm laser at 0.5 W/cm^2 for 5 min. Groups without nanoparticles and with LUGCF-2:1 (no laser irradiation) were used as controls. After 2 h incubation, the cells were washed and fixed with 4% paraformaldehyde for 15 min before confocal microscopy fluorescence images (λ_{ex} = 460 nm, λ_{em} = 530 nm) by a fluorescence microscope (Olympus BX61 light microscope). For quantitative CO analysis by flow cytometry, HCT116 cells (1 × 10^5) were incubated in 24-well plates, and the same procedure was repeated. Cells were eventually washed three times and harvested in 150 μL of flow cytometry staining buffer for flow cytometry (Beckman Coulter FC 500).

For intracellular NO measurement in HCT116 cells, LUGCF-2:1 containing 45 μmol of GSNO and 10 μmol of NO probe was used, and the same procedure used for CO detection was employed for both qualitative and quantitative NO detection. The fluorescence images were captured at λ_{em} = 590 nm.

2.6. Intracellular ROS Detection. Upon CO/NO release in HCT116 cells, ROS probe, 10 μmol 2′,7′-dichlorodihydrofluorescein diacetate (DCFH-DA), was used to determine the intracellular ROS level. Qualitative ROS determination was performed by cell imaging (λ_{ex} = 488 nm, λ_{em} = 530 nm). HCT-116 cells (1 × 10^5 cells/well) were incubated in 12-well plates with coverslips at the bottom for 24 h. The cell culture media were replaced with fresh ones containing 10/5 μg/mL of GSNO/CORM in LUGF, LUCF, and LUGCF-2:1 nanoformulations and further incubated for 4 h. Then, the media were replaced with fresh media containing the ROS probe. For the laser irradiation groups, cells were irradiated with an 808 nm laser for 5 min at 0.5 W/cm^2. After 30 min of incubation, cells were washed three times with PBS and then fixed with 4% paraformaldehyde for 15 min. Fluorescence imaging of cells treated with only the ROS probe was employed as a control group. For the quantitative analysis of the ROS level, cells were treated in the same way for flow cytometry. The cells were incubated in 24-well plates at a density of 1 × 10^5 cells/well and cells were finally washed thrice, trypsinized, and collected in 150 μL of FACS buffer for flow cytometry analysis through detecting DCF fluorescence (λ_{ex} = 488 nm, λ_{em} = 525 nm).

2.7. In Vitro Apoptosis Assay. The apoptotic effect of the nanoformulations was evaluated in HCT116 cells through flow cytometry analysis. Annexin V-fluorescein isothiocyanate (FITC) apoptosis detection kit (BD Biosciences Pharmingen) was employed to determine the cell apoptosis. Briefly, cells at the density of 1 × 10^5 cells/well were seeded in 24-well plates for 24 h. The cells were then treated with media containing LUGCF-2:1 (IC50: 3.4/1.7 μg/mL of GSNO/CORM, calculated from the MTT assay). After 4 h of nanoparticle incubation, media for all groups were replaced with fresh ones, followed by the 808 nm laser irradiation at 0.5 W/cm^2 for 5 min for groups LUGF + L, LUCG + L, and LUGCF-2:1 + L. The cells

https://doi.org/10.1021/acsami.3c13165
ACS Appl. Mater. Interfaces 2023, 15, 56796−56806

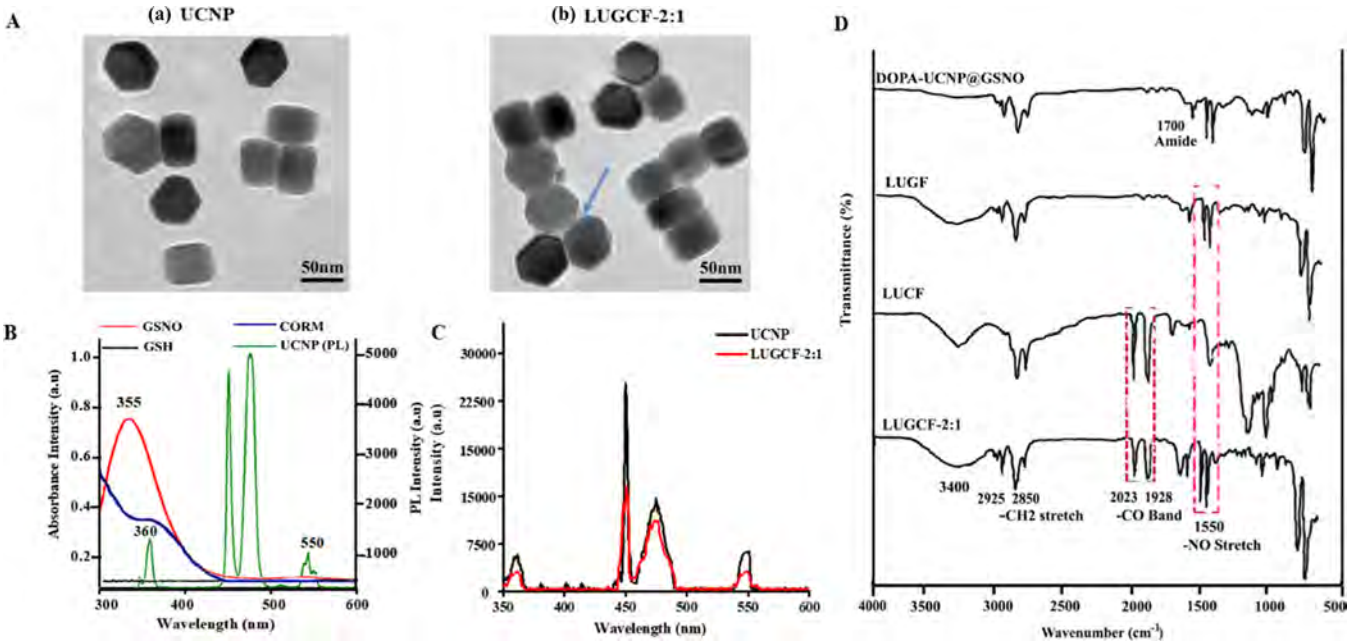

Figure 1. Particle characteristics. (A) TEM images of (a) UCNPs and (b) LUGCF-2:1 nanoparticles. Arrow shows the lipid layer. (B) UV absorbance spectra of aqueous GSH, GSNO, and CORM with photoluminescence spectra (980 nm, 1 W/cm^2) of core−shell UCNPs dispersed in hexane. (C) Photoluminescence spectra (808 nm, 1 W/cm^2) of UCNPs dispersed in cyclohexane and LUGCF-2:1 in HEPES buffer. (D) FTIR spectra of various intermediary and final materials during synthesis.

Table 1. Particle Characteristics of Lipid Nanoformulations

formulations	hydrodynamic diameter (nm)	zeta potential (mV)	polydispersity index	drug loading (wt %)	loading efficiency (%)
Lip/UCNP/FA (LUF)	102 ± 3	−7.4 ± 0.4	0.20 ± 0.02		
Lip/UCNP@GSNO/FA (LUGF)	134 ± 3	−6.1 ± 0.5	0.23 ± 0.08	9.33	70.0
Lip/UCNP/CORM/FA (LUCF)	133 ± 1	−1.0 ± 0.3	0.23 ± 0.11	9.92	74.5
Lip/UCNP@GSNO/CORM/FA (LUGCF-1:1)	132 ± 1	−0.8 ± 0.4	0.21 ± 0.03	4.60/4.59[a]	69.0/68.9[a]
Lip/UCNP@GSNO/CORM/FA (LUGCF-2:1)	139 ± 2	−1.3 ± 0.1	0.27 ± 0.03	4.60/9.10[a]	73.4/73.6[a]
Lip/UCNP@GSNO/CORM/FA (LUGCF-3:1)	137 ± 4	−1.8 ± 0.4	0.23 ± 0.04	4.59/13.8[a]	78.1/73.6[a]
Lip/UCNP@GSNO/CORM/FA (LUGCF-4:1)	139 ± 3	−2.5 ± 0.6	0.27 ± 0.11	4.59/18.4[a]	82.6/82.8[a]

[a]Corresponding drug loading and loading efficiency values of CORM and GSNO in LUGCF, respectively.

were further incubated for 24 h, triplatinized, and centrifuged at 300*g* for 4 min. After washing with 500 μL of cold PBS two times, the cells were resuspended in 100 μL of binding buffer. Then, the cells were stained with 5 μL of an Annexin V-FITC solution and 5 μL of a propidium iodide (PI) solution for another 20 min in the dark. The cells were diluted with 1× binding buffer (400 μL) and analyzed by flow cytometry for at least 1 × 10^5 cells per sample. The population of cells in different quadrants (late apoptotic on the top right, early apoptotic on the bottom right corner, and necrotic cells on the top left side) were analyzed using the quadrant statistics with respect to the untreated control groups stained with Annexin V−PI only.

2.8. In Vivo Therapeutic Effect. All animal experiments were conducted following the institutional guidelines for animal experimentation using the animal-use protocols approved by The University of Queensland's Animal Ethics Committee (AIBN/224/18). Female BALB/c mice (6−8 week old) were housed and provided with unrestricted access to water and food throughout the study. Tumor xenografts in mice were achieved by subcutaneous injection of CT26 cells at a density of 2 × 10^6 in 100 μL of FBS-free cell culture medium on the right flank. The size of tumor and body weight were monitored daily, and tumor volume (V) was calculated using the formula: $V = L \times W^2/2$ (L and W represent the tumor's longest and the shortest dimensions).

Mice were randomly divided into five groups (n = 5) after the respective tumor volume reached ∼100 mm^3. The mice were administered with PBS control, LUGF, LUGF + L, LUCF + L, LUCGF, and LUGCF-2:1 + L by intravenous injection of nanoformulations containing 10 mg/kg of GSNO and/or 5 mg/kg of CORM per dose and 7.5 mg/kg each for LUGCF-1:1 per dose. The drug administration was conducted on days 0, 3, 6, and 9 with postinjection irradiations at 12 h (808 nm, 0.5 W/cm^2 for 5 min).

The therapeutic efficacy was evaluated by tracking the tumor volume and body weight of all mice. After 2 days of the final administration, mice were sacrificed, and the weight of tumors was measured for further analysis. Major organs were also excised for H&E staining to examine the in vivo safety of nanoformulations. Microscopic imaging by an Olympio BX61 microscope was employed to visualize the tissues after staining.

Nanoparticle accumulation at the tumor site was performed with two groups of animals containing three mice. Mice were injected with LUGCF-2:1 nanoformulation, and the control group received saline. All mice were sacrificed after 24 h of injection, and their tumors were harvested and digested for Mn content analysis. The in vivo gas

https://doi.org/10.1021/acsami.3c13165
ACS Appl. Mater. Interfaces 2023, 15, 56796−56806

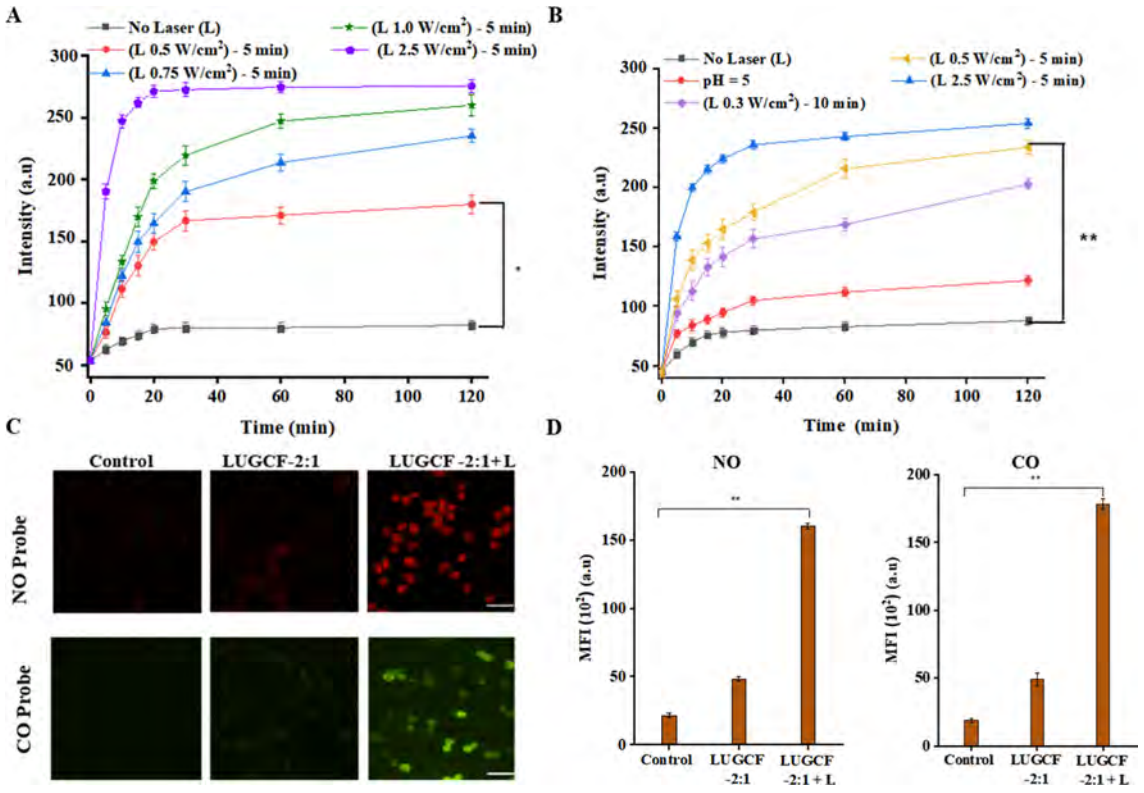

Figure 2. NIR-responsive gas release from the LUGCF-2:1 nanoparticles. Profiles of CO (A) and NO (B) release from the LUGCF-2:1 nanoformulation with different light release conditions. COFP (λ_{ex} = 450 nm, λ_{em} = 530 nm) and NOFP (λ_{ex} = 450 nm, λ_{em} = 600 nm) were used for CO and NO detection, respectively. Fluorescent imaging (C) and flow cytometry analyses (D) of CO and NO release in HCT116 cells. Nanoparticles were replaced at 4 h before treatment with a laser (0.5 W/cm^2) for 5 min. Scale bar = 50 μm.

release and ROS generation in CT26 tumor tissue were also investigated. When the tumors grew to 100 mm^3, mice were intravenously injected with 100 μL of saline as the control group or LUGCF-2:1 formulation containing 10 mg/kg of GSNO and 5 mg/kg of CORM, followed by injection of 50 μL of probe (2 mM) after 10 h. In vivo CO and NO release and ROS generation in the tumor tissues were quantitatively assessed after 12 h upon irradiation prior to imaging.

3. RESULTS AND DISCUSSION

3.1. Characteristics of Therapeutic Gas-Loaded Nanoformulations (LUGCF). In this work, a lipid nanoplatform coloaded with two gas-releasing molecules (NO and CO) for NIR light-responsive release and synergistic cancer therapy was successfully synthesized (Scheme 1). First, OA-capped $NaYF_4$:Yb, Tm, Ho@$NaYF_4$:Nd core−shell UCNPs (UCNPs) had an average particle size of around 55 nm (Figure 1A). Similar to our previous report,[49,50] the hexagonal morphology of core UCNPs was maintained after shell coating (Figure 1A). The core nanoparticles alone absorbed 980 and 808 nm NIR via Nd's absorbance.[53] As shown in Figure 1B, CORM and GSNO in HEPES buffer displayed UV absorptions at λ_{max} = 365 and 350 nm, respectively.

The intermediary amphiphilic nanoparticle named DOPA-UCNP@GSNO was easily incorporated into lipid mixtures containing amphiphilic CORM. In this nanoformulation structure, the amphiphilic GSNO was capped on OA-free UCNPs through the coordination and electrostatic attraction of carboxylic acid (−COOH) to lanthanide ions.[54] The hydrophilic UCNP@GSNO combination was successfully decorated with lipids (DOPA) containing $-HPO_3^{2-}$ functional groups with comparable UCNP binding ability as the second layer ligand.[55] After lipid encapsulation, hexagonal UCNPs were surrounded by a thin layer of lipids (Figure 1A), further confirming the incorporation of lipids and gas-releasing molecules. As shown in Figures 1C and S1, slightly reduced PL intensity (red curve) was observed for the LUGCF-2:1 formulation in HEPES buffer due to the quenching by water molecules in comparison to that in cyclohexane. The characteristic emission at 360 nm upon NIR laser irradiation could trigger release of both gas molecules. Apart from UV emission, the absorbance of GSNO in the visible region (550 nm) was also considered for NO release and thus Ho was introduced in UCNPs to produce a characteristic emission at 550 nm (Figure 1C). These emissions could be induced by both 980 and 808 nm light excitations (Figure S1).

Figure S2 presents FTIR spectra of the starting materials and intermediates of the LUGCF-2:1 nanoformulation, confirming that such a composite structure was successfully constructed. The $-CH_2$ stretching vibrations in OA-coated UCNPs were detected at 2925 and 2856 cm^{-1}. After treatment with $NOBF_4$, a new IR peak at 1100 cm^{-1} was detected, representing the presence of $-BF_4$ (from $NOBF_4$) on the surface. The peak at 1550 cm^{-1} was attributed to −NO in GSNO as compared to standard GSH.[56] This characteristic peak was also detected in UCNP@GSNO as compared to UCNP@GSH. As displayed in Figure 1D, the differences between formulated nanomedicines were prominent. The −NO stretching vibration and amide and amine vibrations were all seen in the FTIR spectrum of LUGF, and the −CO bands (2023 and 1928 cm^{-1}) were observed in the FTIR spectrum of LUCF, confirming the successful encapsulation of GSNO and

https://doi.org/10.1021/acsami.3c13165
ACS Appl. Mater. Interfaces 2023, 15, 56796−56806

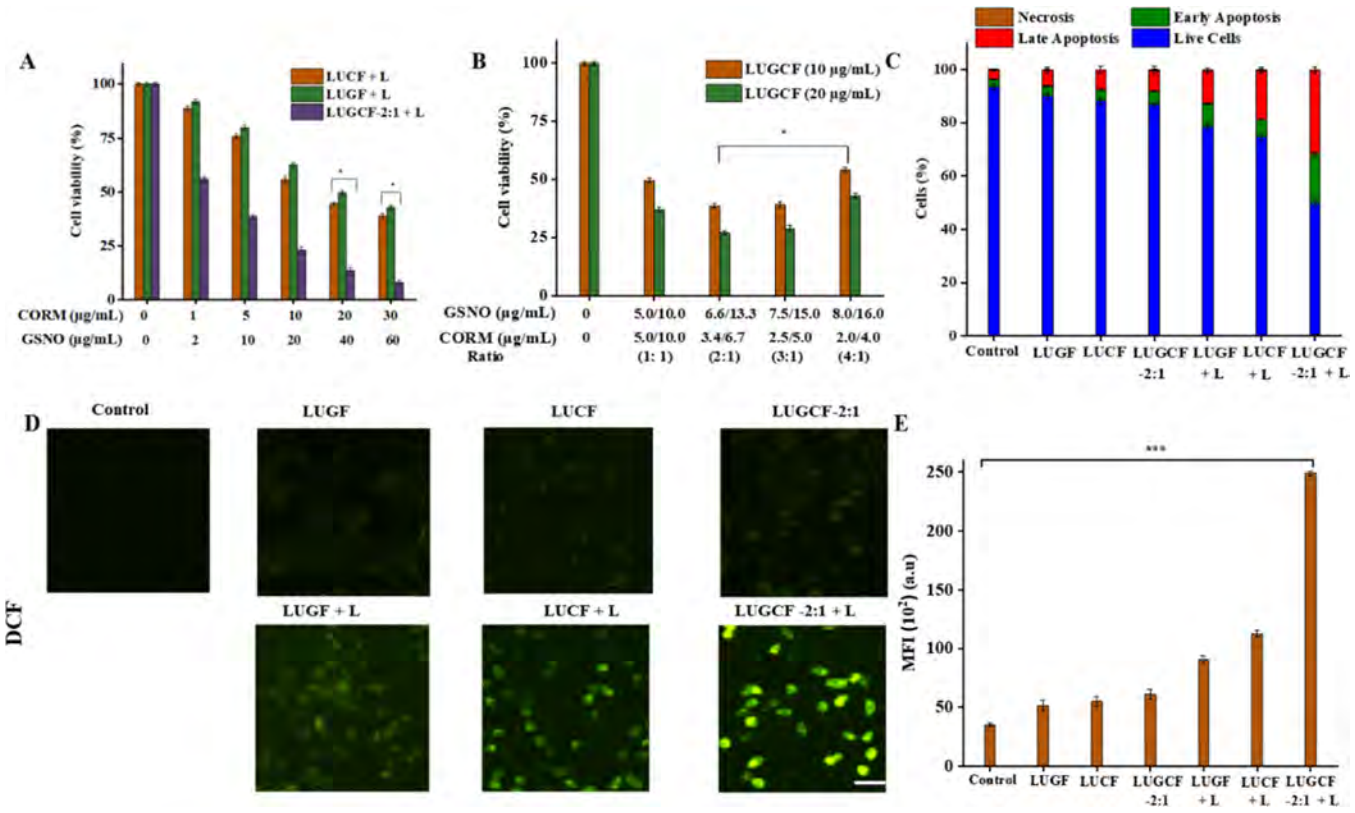

Figure 3. In vitro cytotoxicity studies. (A) Cell viability assay of LUGF, LUCF, and LUGCF-2:1 with laser (L) irradiation in HCT116 cells. (B) MTT assay was performed for different ratios and combinations of LUGCF nanoformulation at 10 and 20 μg/mL in HCT116 cells with light irradiation. (C) Cell apoptosis assay of various formulations showing the apoptotic and necrotic profiles by PI-Annexin V staining of HCT116 cells harvested and stained after treatment for 24 h of treatment. (D) HCT116 cells' fluorescence images of DCFH-DA indicating the qualitative amount of intracellular ROS (λ_{ex} = 450 nm laser line and λ_{em} = 530). (E) Quantitative flow cytometry analysis of ROS contents in HCT116 cells (λ_{ex} = 488 nm laser line and λ_{em} = 525). All nanoparticles were replaced with fresh media after 4 h, and irradiation groups (+L) were treated with an 808 nm light at 0.5 W/cm^2 for 5 min. Scale bar = 50 μm.

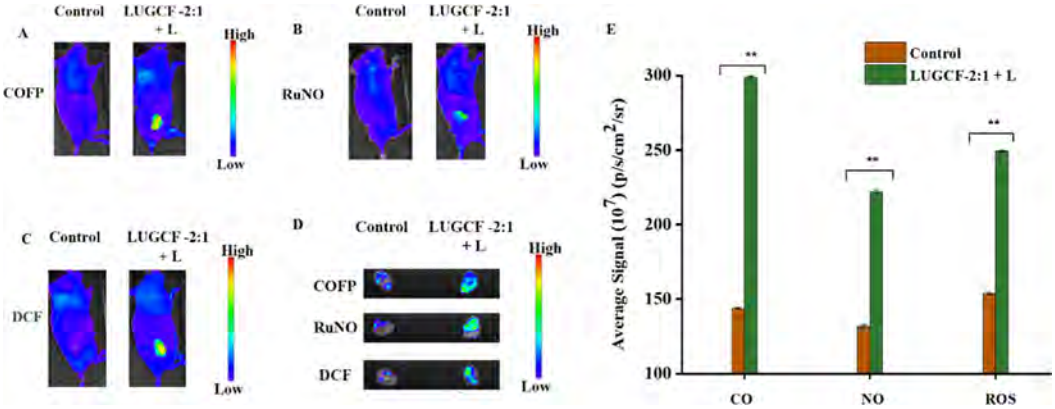

Figure 4. Gas release mechanism and ROS detection. (A) In vivo detection of CO gas after 12 h of administration and irradiation detected by COFP fluorescence. (B) In vivo detection of NO gas after 12 h of administration and irradiation detected by Ru−NO probe fluorescence. (C) In vivo detection of ROS after 12 h of administration and irradiation detected by DCFH-DA fluorescence. (D) Ex vivo detection of COFP, RuNO probe, and DCFH-DA ROS probe. (E) Fluorescence radiance intensity of signals of harvested tumors. Light irradiation was performed at a rate of 0.5 W/cm^2 for 5 min.

CORM, respectively. These respective signals were maintained for dual pro-drug-loaded nanoformulations (LUGCF-2:1), suggesting that a certain amount of GSNO and CORM was simultaneously incorporated into the lipid formulations.

Table 1 summarizes the physicochemical characteristics for prepared formulations. The hydrodynamic diameter of all lipid nanoparticles was mainly in the range of 130−140 nm, suggesting their suitability for cellular uptake and tumor accumulation. LUGCF nanoparticles with both GSNO and CORM gas-releasing molecules (mass ratio from 1:1 to 4:1) had the similar zeta potential (−1.0 ± 0.3 mV to −2.5 ± 0.6 mV) but slightly higher than that of LUF and LUGF, attributed to the incorporation of positive CORM molecules. Note that all nanoparticle formulations contained tumor-

https://doi.org/10.1021/acsami.3c13165
ACS Appl. Mater. Interfaces 2023, 15, 56796−56806

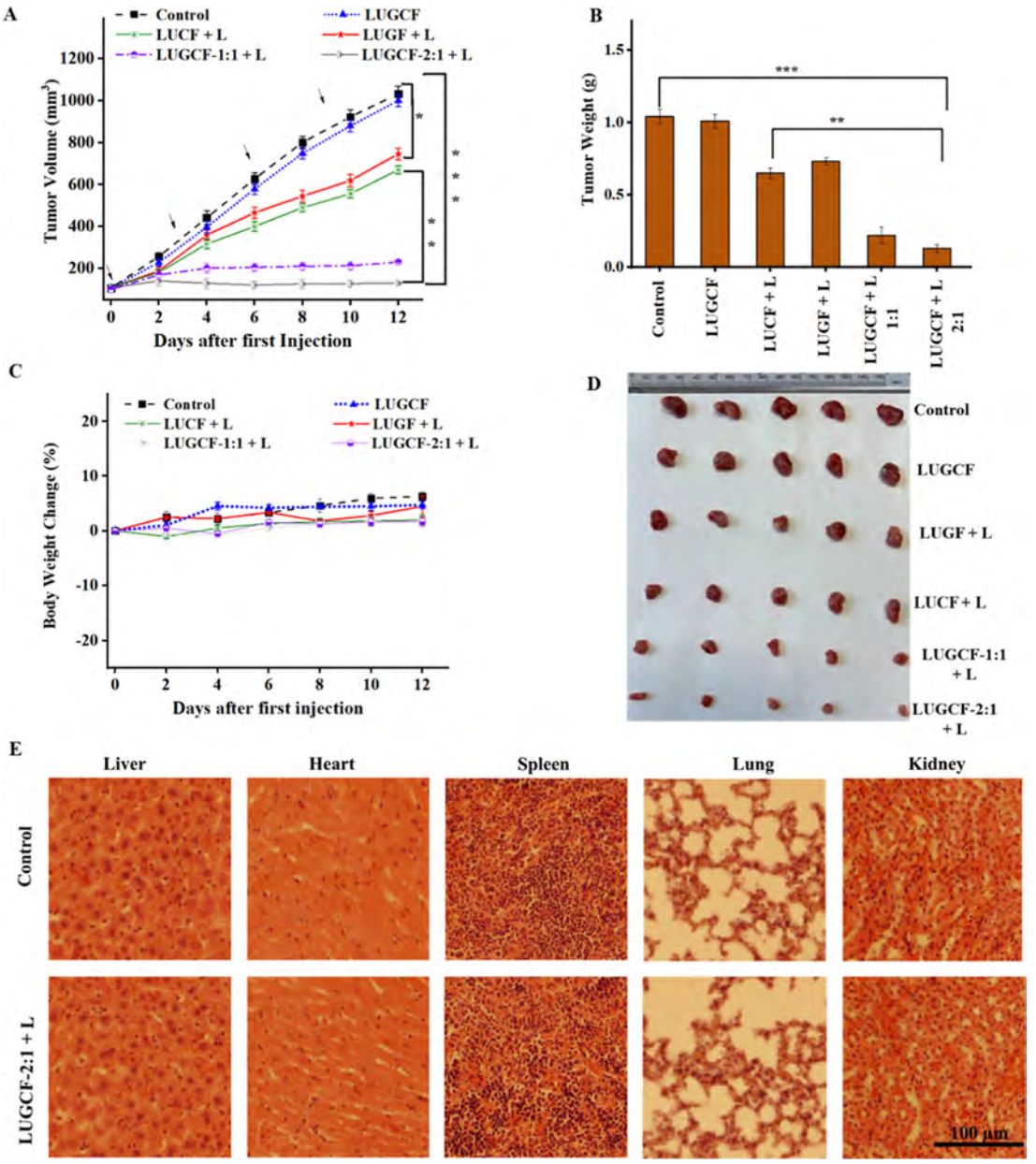

Figure 5. In vivo therapeutic effect. (A) Changes of tumor's volume during the treatment. (B) Weight of tumor after 12 days. (C) Average body weight of mice during the treatment. (D) Images of tumors harvested at 12 days after treatment with different nanoformulations; intravenous injection at day 0, 3, 6, and 9 at 10 mg/kg of GSNO and 5 mg/kg of CORMs per dose or 7.5 mg/kg each for LUGCF-1:1 per dose, and light irradiation at 12 h after each injection (808 nm, 0.5 W/cm^2 for 5 min) for irradiation groups. (E) H&E staining indicates the histopathological status of major organs after animal treatment with LUGCF-2:1 + L on day 12. Scale = 100 μm.

targeting ligand folic acid (FA) for enhanced delivery as reported previously.[57] Further note that the colloidal stability of LUGCF-2:1 nanoparticles in HEPES buffer and DMEM (mimicking biological fluids) was confirmed by the unchanged particle size and zeta potential during incubation at 4 °C for 12 days (Figure S3).

Four LUGCF formulations had the loading efficiency of GSNO and CORM at 70−80% individually or together (Table 1). As detailed in Table 1, the CORM was maintained at 4.6 wt % while GSNO varied between 4.6, 9.1, 13.8, and 18.4% in these LUGCF nanoparticles.

3.2. NIR-Triggered Gas Release. NIR-mediated gas release was detected by the characteristic turn off−on properties of COFP and NOFP. First, UCNPs containing Tm-doping ($NaYF_4$:Yb, Tm@$NaYF_4$:Nd, Tm/UCNP), Ho-doping ($NaYF_4$:Yb, Ho@$NaYF_4$:Nd, Ho/UCNP), and codoping (Tm/Ho/UCNPs) at 0.5% Tm and 1% Ho were prepared. $NaYF_4$:Yb, Ho, and Tm@$NaYF_4$:Nd were conjugated with GSNO and DOPA for comparison of NO release efficacy. Figure S4A displays the effect of codoping Ho (550 nm emission) into Tm UCNPs (360 nm emission) on NO release from intermediary DOPA-UCNP@GSNO nanoparticles. Tm/UCNP-mediation with the release of NO from GSNO obviously produced a desirable fluorescence intensity (λ_{ex} = 600 nm), which was slightly enhanced by employing Tm/Ho/UCNPs. However, the detection of NO released from Ho/UCNPs was relatively low (35%) as compared to other groups under the same conditions. The codoping (Tm/Ho/UCNPs)

https://doi.org/10.1021/acsami.3c13165
ACS Appl. Mater. Interfaces 2023, 15, 56796−56806

seems optimal for this study because CORM absorbs photons at 360 nm, while GSNO at both 350 and 550 nm. In further comparison,similar fluorescence intensity was observed when an 808 or a 980 nm NIR laser was employed to irradiate LUGF (Figure S4B), which means UCNPs are very similarly responsive to both lights, and the 808 nm laser was selected.

As depicted in Figure 2A, CO release seemed rapid within 10 min after laser irradiation, and the delivery system moderately slowed the gas diffusion across lipid bilayers in the coming 10−20 min as observed in other CO detection assay.[58] If the release upon laser irradiation at 2.5 W/cm^2 was regarded as the maximum after 120 min of incubation, ∼50% of the maximum CO level was released upon an 808 nm laser irradiation at 0.5 W/cm^2 for 5 min after 30−40 min of incubation (Figure 2A). After irradiation, no significant CO release was detected from control and irradiated samples until 180 h (Figure S5C). After 120 min of incubation of LUGCF-2:1 in the presence of COFP, repeated irradiation (0.5 W/cm^2 for 5 min) released CO from ∼50 to ∼90% of the maximum level in the subsequent 60 min (120−180 min, Figure S5A). Note that the second irradiation at 2.5 W/cm^2 did not release any more CO, indicating that one 808 nm laser irradiation at 2.5 W/cm^2 for 5 min triggered the release of all possible CO molecules (Figure 2A).

Similar to the CO release profile, NO release also showed a laser power-dependent pattern (Figure 2B). A rapid burst release of NO in the first 30 min was observed upon laser irradiation at both 0.5 and 2.5 W/cm^2 for 5 min, and there was about 10−15% more NO released in 60−120 min. A repeated irradiation at 0.5 W/cm^2 for 5 min after 120 min of incubation further released NO molecules to be close to the maximum amount (Figure S5B). Clearly, further incubation after the second irradiation did not release any NO from 180 min to 180 h (Figure S5D). More interestingly, 60−70% of the maximum NO was released upon irradiation at 0.3 W/cm^2 for 10 min. These data suggest that the laser power at 0.5 W/cm^2 for 5 min was suitable for subsequent experiments to simultaneously release moderate amounts of CO and NO for therapeutic action. In addition, there was a slightly more NO release from GSNO in buffers at physiological pH below 5 (mimicking endosome/lysosome and tumor tissue microenvironment) in comparison with that in pH 7.4 medium as the formation of GSNO from GSH occurs in pH below 5 and is reversible in the presence of excess acid (Figure 2B).[59]

Figure 2C shows the qualitative detection of intracellular CO and NO release after the cellular uptake of LUGCF-2:1. In the absence of LUGCF-2:1 formulation, HCT116 cells produced undetectable NO and CO fluorescence. In the absence of irradiation after 4 h of incubation with LUGCF-2:1, weak visible fluorescence was observed. In sharp contrast, NIR irradiation at 0.5 W/cm^2 for 5 min produced much more intense fluorescence in cells for both the NO and the CO probes. As illustrated in Figure 2D, the observed fluorescence intensity of irradiated cells via two probes was significantly higher than that of other treatments (Figure S6A,B). These quantitative and qualitative data confirm that LUGCF-2:1 was successfully taken up by cells, and the internalized formulations produced gases in detectable quantities in cells upon laser irradiation.

3.3. In Vitro Cancer Gas Therapy. Cell viability assay, PI-Annexin V apoptosis, and ROS detection were employed to determine the optimal combination and therapeutic mechanism. Figure 3A shows that single therapeutic nanomedicines (LUCF and LUGF) exhibited a dose-dependent cytotoxicity to HCT116 upon an 808 nm laser irradiation at 0.5 W/cm^2 for 5 min, with the IC_{50} value being 12.9 (CORM) and 41.6 (GSNO) μg/mL (Table S4), respectively. In comparison, LUCF and LUGF themselves showed very limited cytotoxicity to HCT116 cells (IC50 being 198.1 and 211.3 μg/mL, respectively; Figure S7A and Table S4). Co-loading HCT116 cells with GSNO and CORM at a mass ratio of 2:1 (LUGCF-2:1) without laser irradiation moderately reduced the cell viability at high doses (e.g., 57.9% cell viability at 60/30 μg/mL of GSNO/CORM) (Figure S7A), with their combined IC50 being 93.0/46.5 μg/mL (Table S4). In sharp contrast, laser irradiation at 0.5 W/cm^2 for 5 min efficiently induced cell death (Figure 3A), remarkably reducing the IC50 to 3.4/1.7 μg/mL in the GSNO/CORM combination (LUGCF-2:1).

To optimize the GSNO/CORM mass ratio in LUGCF for enhanced cytotoxicity, the total GSNO/CORM concentration was fixed at 20 and 10 μg/mL with their mass ratios varying from 1:1 to 4:1, respectively. As shown in Figure 3B, the higher dose (20 μg/mL) reduced the HCT116 cell viability by 10−15% in comparison to the lower dose (10 μg/mL) in all corresponding combinations upon an 808 nm laser irradiation. Relatively, both 2:1 and 3:1 combination showed a similarly higher cytotoxicity, e.g., killing 61.2%/72.9% and 60.7%/71.1% HCT116 cells at 10/20 μg/mL of the total doses, respectively. This cytotoxicity is significantly higher than that of LUGCF at the GSNO/CORM mass ratio of 1:1 and 4:1.

In consistence, the synergistic effect of two gas-releasing molecules in LUGCF-2:1 combination was analyzed by estimating the combination index (CI). As listed in Table S3, the CI was 1.85 and 1.84 for 2:1 and 3:1 LUGCF combinations, respectively, remarkably higher than that for 1:1 (CI = 1.26) and 4:1 (CI = 1.34) combinations. In contrast, an additive effect (CI = 0.94−1.02) was observed for treatments with all combinations without laser irradiation (Table S4). On the other hand, about 25% of cell death was observed for both 2:1 and 3:1 LUGCF at 20 μg/mL of GSNO/CORM, and slightly lower cell death was observed for both 4:1 and 1:1 combination (∼19%) without light irradiation (Figure S8A). Very interestingly, this similar cell viability was observed in both human (HCT116) and mice colon cancer cells (CT26 cells) with or without light irradiation (Figure S8B−D), which suggests that the LUGCF nanoformulation is similarly effective in both colon cancer cells. In comparison, the cell viability of healthy kidney cells (HEK293T) was not affected by this combination treatment at much higher concentrations (Figure S7B), e.g., 85.3% cell viability at 60/30 μg/mL of GSNO/CORM, suggesting a much lower side effect of LUGCF nanomedicine to normal cells.

PI-Annexin V flow cytometry apoptosis analysis indicates that LUGCF-2:1 induced more early and late apoptotic cells as compared to other groups at 3.4/1.7 μg/mL GSNO/CORM with or without light irradiation (Figure 3C). As shown in Figure S9, LUGF, LUCF, and LUGCF induced 9.7, 11.5, and 12.9% cell death, while the total cell death was increased to 25.1% (LUCF) and 21.0% (LUGF) upon light irradiation. As expected, LUGCF-2:1 + L induced 18.7% early apoptosis and 31.7% late apoptosis (50.4% total cell death), much more efficiently than the single gas nanomedicine, probably attributed to the synergy.

Consistently, a pivotal cancer-killing mechanism of therapeutic gases has been confirmed to involve CO- and NO-induced ROS. As indicated in Figure 3D,E, LUGF, LUCF, and

https://doi.org/10.1021/acsami.3c13165
ACS Appl. Mater. Interfaces 2023, 15, 56796−56806

LUGCF-2:1 alone produced very limited ROS without light irradiation. Light irradiation of LUGF and LUCF induced relatively strong intracellular ROS signals, while a significantly higher fluorescence signal was observed for LUGCF-2:1, indicating a strong synergistic effect of simultaneously released CO and NO on the production of ROS/RNS species. As proposed previously, released NO further produces $NO^{\bullet}$, $ONOO^{-}$, and other forms of RNS whereas CO also produces ROS in the intracellular level for enhanced cancer therapy.[60]

3.4. In Vivo Photoresponsive Gas Therapy. In situ gas release and intratumoral ROS generation were assessed in mice using one animal selected from all groups. As seen in Figure 4A, animals treated with LUGCF-2:1 + L produced strong COFP fluorescence signals at the tumor site as compared to the control group receiving just saline and the COFP probe. A similar phenomenon was observed for the NOFP probe with the same formulation treatment (Figure 4B). The ROS signal (DCF) was also clearly observed in mice treated with the LUGCF-2:1 formulation upon light irradiation (Figure 4C). Consistently, harvested tumor tissues from animals treated with LUGCF-2:1 + L showed much higher signals than the control groups (Figure 4D) as quantified in Figure 4E. Very obviously, the control signals were significantly lower than the LUGCF + L treatment group, and the ROS detection was also confirmed by the high signal. These data suggest that gases were responsively released in tumor tissues after NIR laser irradiation and released gases significantly contributed to ROS generation for in situ cancer gas therapy.

The therapeutic effect of the combined GSNO/CORM therapy in the lipid nanoformulations was then assessed by intravenous injection into CT26 tumor-bearing mice. As seen in Figure 5A, injections of LUGCF-2:1 did not inhibit tumor growth (dashed blue line). Relatively, treatments with LUCF + L and LUGF + L provided a moderate degree of tumor inhibition, as compared to the control group, by 35.1% ± 1.9% and 27.8% ± 2.7%, respectively, at day 12. Notably, both 2:1 and 1:1 formulations (LUGCF-2:1 + L and LUGCF-1:1 + L) significantly inhibited tumor growth by 87.5% ± 0.7% and 77.7% ± 0.8%, respectively, at day 12 (Figure 5A). In comparison, LUGCF-2:1 more efficiently inhibited the tumor growth than LUGCF-1:1, consistent with the in vitro data (Figure 3A). In specific, the tumor size was not increased during the whole treatment period in the LUGCF-2:1 + L group. The weight of collected tumor tissues was consistent with the tumor volume at day 12 for all groups of mice, being reduced by 87.5% ± 1.5%, 78.8% ± 5.3%, 37.5% ± 3.5%, and 29.8% ± 2.6% for LUGCF-2:1 + L, LUGCF-1:1 + L, LUCF + L, and LUGF + L groups, respectively, in comparison with the control group (Figure 5B). The efficient therapeutic effect of GSNO and CORM in the combination formulation under NIR irradiation for tumor growth inhibition can be attributed to their synergy at the carefully selected mass ratio.

No loss of body weight in all groups was observed throughout the study (Figure 5C). The tumor size increase in the control group likely resulted in a minor net weight gain. Furthermore, comparing with the control group, there were no significant morphological changes in the tissue histopathology of excised organs (Figure 5E). These data demonstrate the good biosafety and biocompatibility of these nanoformulations during the treatment.

4. CONCLUSIONS

In this research, we successfully developed a lipid drug delivery system capable of loading two gas-releasing molecules (CORM and GSNO) and targeting tumor cells with folate. UCNPs were engineered and incorporated to mediate NIR to UV light conversion for a responsive gas release. The formulation LUGCF-2:1 was confirmed to be relatively stable in biological media. In vitro and in vivo data demonstrated that significant amounts of CO and NO gases were released via an 808 nm NIR irradiation. The optimal mass ratio of two gas pro-drug molecules encapsulated act synergistically to inhibit HCT116 and CT26 colon cancer cell growth, particularly in the mouse model upon an 808 nm light irradiation at 0.5 W/cm^2 for 5 min. In summary, this nanoplatform provides a new strategy for codelivery of molecules containing gasotransmitters for synergistic cancer therapy using noninvasive release triggers such as NIR lights.

■ ASSOCIATED CONTENT

Supporting Information

The Supporting Information is available free of charge at https://pubs.acs.org/doi/10.1021/acsami.3c13165.

Optical characterization, CO/NO release profile and corresponding flow cytometry analyses, ROS generation, MTT assay, cell apoptosis analyses, and additional experimental methods (PDF)

■ AUTHOR INFORMATION

Corresponding Authors

Run Zhang − *Australian Institute for Bioengineering and Nanotechnology, The University of Queensland, Brisbane, Queensland 4072, Australia;* orcid.org/0000-0002-0943-824X; Email: r.zhang@uq.edu.au

Zhi Ping Xu − *Australian Institute for Bioengineering and Nanotechnology, The University of Queensland, Brisbane, Queensland 4072, Australia;* orcid.org/0000-0001-6070-5035; Email: gordonxu@uq.edu.au

Authors

Yaw Opoku-Damoah − *Australian Institute for Bioengineering and Nanotechnology, The University of Queensland, Brisbane, Queensland 4072, Australia*

Hang T. Ta − *Australian Institute for Bioengineering and Nanotechnology, The University of Queensland, Brisbane, Queensland 4072, Australia; School of Environment and Science and Queensland Micro and Nanotechnology Centre, Griffith University, Brisbane, Queensland 4111, Australia;* orcid.org/0000-0003-1188-0472

Complete contact information is available at: https://pubs.acs.org/10.1021/acsami.3c13165

Author Contributions

The manuscript was written through contributions of all authors. All authors have given approval to the final version of the manuscript.

Funding

This work was financially supported by the Australian Research Council (ARC) Discovery Projects (DP190103486) and National Health and Medical Research Council (APP1175808).

Notes

The authors declare no competing financial interest.

■ ACKNOWLEDGMENTS

Y.O.−D. gratefully acknowledges the Australian Government Research Training Program Scholarship (RTP). The authors also give thanks to facilities and the technical assistance of the Australian Microscopy & Microanalysis Research Facility at the Centre for Microscopy and Microanalysis (CMM) and Centre of Advanced Imaging, The University of Queensland. This work used the Queensland node of the NCRIS-enabled Australian National Fabrication Facility (ANFF-Q).

■ REFERENCES

(1) Shi, J.; Kantoff, P. W.; Wooster, R.; Farokhzad, O. C. Cancer nanomedicine: progress, challenges and opportunities. *Nat. Rev. Cancer* **2017**, *17* (1), 20−37.
(2) Yao, X.; Yang, B.; Xu, J.; He, Q.; Yang, W. Novel gas-based nanomedicines for cancer therapy. *VIEW* **2022**, *3* (1), 20200185.
(3) Opoku-Damoah, Y.; Zhang, R.; Ta, H. T.; Xu, Z. P. Therapeutic gas-releasing nanomedicines with controlled release: Advances and perspectives. *Exploration* **2022**, *2* (5), 20210181.
(4) Ji, C.; Zheng, X.; Li, S.; Liu, C.; Yin, M. Perylenediimides with Enhanced Autophagy Inhibition for a Dual-Light Activatable Photothermal Gas Therapy. *ACS Appl. Mater. Interfaces* **2023**, *15* (29), 34427−34435.
(5) Yang, N.; Gong, F.; Cheng, L. Recent advances in upconversion nanoparticle-based nanocomposites for gas therapy. *Chem. Sci.* **2022**, *13* (7), 1883−1898.
(6) Motterlini, R.; Otterbein, L. E. The therapeutic potential of carbon monoxide. *Nat. Rev. Drug Discovery* **2010**, *9* (9), 728−743.
(7) Carpenter, A. W.; Schoenfisch, M. H. Nitric oxide release: Part II. Therapeutic applications. *Chem. Soc. Rev.* **2012**, *41* (10), 3742−3752.
(8) Jiang, Y.; Fu, P.; Liu, Y.; Wang, C.; Zhao, P.; Chu, X.; Jiang, X.; Yang, W.; Wu, Y.; Wang, Y.; Xu, G.; Hu, J.; Bu, W. Near-infrared light-triggered NO release for spinal cord injury repair. *Sci. Adv.* **2020**, *6* (39), No. eabc3513.
(9) Mohapatra, A.; Mondal, J.; Sathiyamoorthy, P.; Mohanty, A.; Revuri, V.; Rajendrakumar, S. K.; Lee, Y.-K.; Park, I.-K. Thermosusceptible Nitric-Oxide-Releasing Nitrogel for Strengthening Antitumor Immune Responses with Tumor Collagen Diminution and Deep Tissue Delivery during NIR Laser-Assisted Photoimmunotherapy. *ACS Appl. Mater. Interfaces* **2023**, *15* (11), 14173−14183.
(10) Verma, A.; Hirsch, D. J.; Glatt, C. E.; Ronnett, G. V.; Snyder, S. H. Carbon Monoxide: a Putative Neural Messenger. *Science* **1993**, *259* (5093), 381−384.
(11) Yang, T.; Zelikin, A. N.; Chandrawati, R. Progress and Promise of Nitric Oxide-Releasing Platforms. *Adv. Sci.* **2018**, *5* (6), 1701043.
(12) Zhang, X.; Guo, Z.; Liu, J.; Tian, G.; Chen, K.; Yu, S.; Gu, Z. Near infrared light triggered nitric oxide releasing platform based on upconversion nanoparticles for synergistic therapy of cancer stem-like cells. *Sci. Bull.* **2017**, *62* (14), 985−996.
(13) Kang, Y.; Kim, J.; Park, J.; Lee, Y. M.; Saravanakumar, G.; Park, K. M.; Choi, W.; Kim, K.; Lee, E.; Kim, C.; Kim, W. J. Tumor vasodilation by N-Heterocyclic carbene-based nitric oxide delivery triggered by high-intensity focused ultrasound and enhanced drug homing to tumor sites for anti-cancer therapy. *Biomaterials* **2019**, *217*, 119297.
(14) Li, S.; Song, X.; Zhu, W.; Chen, Y.; Zhu, R.; Wang, L.; Chen, X.; Song, J.; Yang, H. Light-Switchable Yolk-Mesoporous Shell UCNPs@MgSiO3 for Nitric Oxide-Evoked Multidrug Resistance Reversal in Cancer Therapy. *ACS Appl. Mater. Interfaces* **2020**, *12* (27), 30066−30076.
(15) Loboda, A.; Jozkowicz, A.; Dulak, J. HO-1/CO system in tumor growth, angiogenesis and metabolism — Targeting HO-1 as an anti-tumor therapy. *Vasc. Pharmacol.* **2015**, *74*, 11−22.
(16) Wegiel, B.; Gallo, D.; Csizmadia, E.; Harris, C.; Belcher, J.; Vercellotti, G. M.; Penacho, N.; Seth, P.; Sukhatme, V.; Ahmed, A.; Pandolfi, P. P.; Helczynski, L.; Bjartell, A.; Persson, J. L.; Otterbein, L. E. Carbon Monoxide Expedites Metabolic Exhaustion to Inhibit Tumor Growth. *Cancer Res.* **2013**, *73* (23), 7009−7021.
(17) Taillé, C.; El-Benna, J.; Lanone, S.; Boczkowski, J.; Motterlini, R. Mitochondrial Respiratory Chain and NAD(P) H Oxidase Are Targets for theAntiproliferative Effect of Carbon Monoxide in Human Airway SmoothMuscle. *J. Biol. Chem.* **2005**, *280* (27), 25350−25360.
(18) Liu, B.; Zhang, X.; Li, J.; Yao, S.; Lu, Y.; Cao, B.; Liu, Z. X-ray-Triggered CO Release Based on $GdW_{10}/MnBr(CO)_5$ Nanomicelles for Synergistic Radiotherapy and Gas Therapy. *ACS Appl. Mater. Interfaces* **2022**, *14* (6), 7636−7645.
(19) Wu, L.; Wang, R. Carbon Monoxide: Endogenous Production, Physiological Functions, and Pharmacological Applications. *Pharmacol. Rev.* **2005**, *57* (4), 585−630.
(20) Vummaleti, S. V. C.; Branduardi, D.; Masetti, M.; De Vivo, M.; Motterlini, R.; Cavalli, A. Theoretical Insights into the Mechanism of Carbon Monoxide (CO) Release from CO-Releasing Molecules. *Chem.—Eur. J.* **2012**, *18* (30), 9267−9275.
(21) Ji, X.; De La Cruz, L. K. C.; Pan, Z.; Chittavong, V.; Wang, B. pH-Sensitive metal-free carbon monoxide prodrugs with tunable and predictable release rates. *Chem. Commun.* **2017**, *53* (69), 9628−9631.
(22) Kang, J.; Li, Z.; Organ, C. L.; Park, C.-M.; Yang, C.-t.; Pacheco, A.; Wang, D.; Lefer, D. J.; Xian, M. pH-Controlled Hydrogen Sulfide Release for Myocardial Ischemia-Reperfusion Injury. *J. Am. Chem. Soc.* **2016**, *138* (20), 6336−6339.
(23) Lo Iacono, L.; Boczkowski, J.; Zini, R.; Salouage, I.; Berdeaux, A.; Motterlini, R.; Morin, D. A carbon monoxide-releasing molecule (CORM-3) uncouples mitochondrial respiration and modulates the production of reactive oxygen species. *Free Radical Biol. Med.* **2011**, *50* (11), 1556−1564.
(24) Jin, Z.; Wen, Y.; Xiong, L.; Yang, T.; Zhao, P.; Tan, L.; Wang, T.; Qian, Z.; Su, B.-L.; He, Q. Intratumoral H_2O_2-triggered release of CO from a metal carbonyl-based nanomedicine for efficient CO therapy. *Chem. Commun.* **2017**, *53* (40), 5557−5560.
(25) Zhang, Y.; Shen, W.; Zhang, P.; Chen, L.; Xiao, C. GSH-triggered release of sulfur dioxide gas to regulate redox balance for enhanced photodynamic therapy. *Chem. Commun.* **2020**, *56* (42), 5645−5648.
(26) Li, S.; Liu, R.; Jiang, X.; Qiu, Y.; Song, X.; Huang, G.; Fu, N.; Lin, L.; Song, J.; Chen, X.; Yang, H. Near-Infrared Light-Triggered Sulfur Dioxide Gas Therapy of Cancer. *ACS Nano* **2019**, *13* (2), 2103−2113.
(27) Bao, X.; Zheng, S.; Zhang, L.; Shen, A.; Zhang, G.; Liu, S.; Hu, J. Nitric-Oxide-Releasing aza-BODIPY: A New Near-Infrared J-Aggregate with Multiple Antibacterial Modalities. *Angew. Chem., Int. Ed.* **2022**, *134* (32), No. e202207250.
(28) Zhang, K.; Xu, H.; Jia, X.; Chen, Y.; Ma, M.; Sun, L.; Chen, H. Ultrasound-Triggered Nitric Oxide Release Platform Based on Energy Transformation for Targeted Inhibition of Pancreatic Tumor. *ACS Nano* **2016**, *10* (12), 10816−10828.
(29) Meyer, H.; Brenner, M.; Höfert, S. P.; Knedel, T.-O.; Kunz, P. C.; Schmidt, A. M.; Hamacher, A.; Kassack, M. U.; Janiak, C. Synthesis of oxime-based CO-releasing molecules, CORMs and their immobilization on maghemite nanoparticles for magnetic-field induced CO release. *Dalton Trans.* **2016**, *45* (18), 7605−7615.
(30) Cheng, J.; He, K.; Shen, Z.; Zhang, G.; Yu, Y.; Hu, J. Nitric Oxide (NO)-Releasing Macromolecules: Rational Design and Biomedical Applications. *Front. Chem.* **2019**, *7*, 530.
(31) Xu, Y.; Fan, M.; Yang, W.; Xiao, Y.; Zeng, L.; Wu, X.; Xu, Q.; Su, C.; He, Q. Homogeneous Carbon/Potassium-Incorporation Strategy for Synthesizing Red Polymeric Carbon Nitride Capable of Near-Infrared Photocatalytic H2 Production. *Adv. Mater.* **2021**, *33* (39), 2101455.
(32) Stubauer, G.; Giuffrè, A.; Sarti, P. Mechanism of S-Nitrosothiol Formation and Degradation Mediated by Copper Ions*. *J. Biol. Chem.* **1999**, *274* (40), 28128−28133.

(33) Prime, T. A.; Blaikie, F. H.; Evans, C.; Nadtochiy, S. M.; James, A. M.; Dahm, C. C.; Vitturi, D. A.; Patel, R. P.; Hiley, C. R.; Abakumova, I.; Requejo, R.; Chouchani, E. T.; Hurd, T. R.; Garvey, J. F.; Taylor, C. T.; Brookes, P. S.; Smith, R. A. J.; Murphy, M. P. A mitochondria-targeted S-nitrosothiol modulates respiration, nitrosates thiols, and protects against ischemia-reperfusion injury. *Proc. Natl. Acad. Sci. U.S.A.* **2009**, *106* (26), 10764−10769.
(34) Sinha, I.; Hannawa, K. K.; Ailawadi, G.; Woodrum, D. T.; Ford, J. W.; Henke, P. K.; Stanley, J. C.; Eagleton, M. J.; Upchurch, G. R. The Nitric Oxide Donor DETA-NONOate Decreases Matrix Metalloproteinase-9 Expression and Activity in Rat Aortic Smooth Muscle and Abdominal Aortic Explants. *Ann. Vasc. Surg.* **2006**, *20* (1), 92−98.
(35) Miller, M. R.; Okubo, K.; Roseberry, M. J.; Webb, D. J.; Megson, I. L. Extracellular Nitric Oxide Release Mediates Soluble Guanylate Cyclase-Independent Vasodilator Action of Spermine NONOate: Comparison with Other Nitric Oxide Donors in Isolated Rat Femoral Arteries. *J. Cardiovasc. Pharmacol.* **2004**, *43* (3), 440−451.
(36) Hiramoto, K.; Ryuno, Y.; Kikugawa, K. Decomposition of N-nitrosamines, and concomitant release of nitric oxide by Fenton reagent under physiological conditions. *Mutat. Res. Genet. Toxicol. Environ. Mutagen.* **2002**, *520* (1−2), 103−111.
(37) Jeong, H.; Park, J.-H.; Shin, J. H.; Yoo, J.-C.; Park, C. Y.; Hong, J. Prolonged Release Period of Nitric Oxide Gas for Treatment of Bacterial Keratitis by Amine-Rich Polymer Decoration of Nanoparticles. *Chem. Mater.* **2018**, *30* (23), 8528−8537.
(38) Sharma, N.; Dhyani, A. K.; Marepally, S.; Jose, D. A. Nanoscale lipid vesicles functionalized with a nitro-aniline derivative for photoinduced nitric oxide (NO) delivery. *Nanoscale Adv.* **2020**, *2* (1), 463−469.
(39) Gao, L.; Dong, B.; Zhang, J.; Chen, Y.; Qiao, H.; Liu, Z.; Chen, E.; Dong, Y.; Cao, C.; Huang, D.; Chen, W. Functional Biodegradable Nitric Oxide Donor-Containing Polycarbonate-Based Micelles for Reduction-Triggered Drug Release and Overcoming Multidrug Resistance. *ACS Macro Lett.* **2019**, *8* (12), 1552−1558.
(40) Zhao, W.; Zhao, Y.; Wang, Q.; Liu, T.; Sun, J.; Zhang, R. Remote Light-Responsive Nanocarriers for Controlled Drug Delivery: Advances and Perspectives. *Small* **2019**, *15* (45), 1903060.
(41) Khaled, R. M.; Friedrich, A.; Ragheb, M. A.; Abdel-Ghani, N. T.; Mansour, A. M. Cytotoxicity of photoactivatable bromo tricarbonyl manganese(I) compounds against human liver carcinoma cells. *Dalton Trans.* **2020**, *49* (27), 9294−9305.
(42) Li, Y.; Gong, T.; Gao, H.; Chen, Y.; Li, H.; Zhao, P.; Jiang, Y.; Wang, K.; Wu, Y.; Zheng, X.; Bu, W. ZIF-Based Nanoparticles Combine X-Ray-Induced Nitrosative Stress with Autophagy Management for Hypoxic Prostate Cancer Therapy. *Angew. Chem., Int. Ed.* **2021**, *60* (28), 15472−15481.
(43) Qian, Y.; Chen, F.; Wang, M.; Sun, Q.; Shao, D.; Li, C. Near-Infrared Light Triggered Intelligent Nanoplatform for Synergistic Chemo-Photodynamic Therapy of Tumor. *Adv. Opt. Mater.* **2023**, *11* (11), 2202060.
(44) Li, Y.; Dang, J.; Liang, Q.; Yin, L. Carbon monoxide (CO)-Strengthened cooperative bioreductive anti-tumor therapy via mitochondrial exhaustion and hypoxia induction. *Biomaterials* **2019**, *209*, 138−151.
(45) Garcia, J. V.; Yang, J.; Shen, D.; Yao, C.; Li, X.; Wang, R.; Stucky, G. D.; Zhao, D.; Ford, P. C.; Zhang, F. NIR-Triggered Release of Caged Nitric Oxide using Upconverting Nanostructured Materials. *Small* **2012**, *8* (24), 3800−3805.
(46) Duan, C.; Liang, L.; Li, L.; Zhang, R.; Xu, Z. P. Recent progress in upconversion luminescence nanomaterials for biomedical applications. *J. Mater. Chem. B* **2018**, *6* (2), 192−209.
(47) Zhang, M.; Liu, X.; Mao, Y.; He, Y.; Xu, J.; Zheng, F.; Tan, W.; Rong, S.; Chen, Y.; Jia, X.; Li, H. Oxygen-Generating Hydrogels Overcome Tumor Hypoxia to Enhance Photodynamic/Gas Synergistic Therapy. *ACS Appl. Mater. Interfaces* **2022**, *14* (24), 27551−27563.
(48) Liu, B.; Li, C.; Yang, P.; Hou, Z.; Lin, J. 808-nm-Light-Excited Lanthanide-Doped Nanoparticles: Rational Design, Luminescence Control and Theranostic Applications. *Adv. Mater.* **2017**, *29* (18), 1605434.
(49) Opoku-Damoah, Y.; Zhang, R.; Ta, H. T.; Amilan Jose, D.; Sakla, R.; Xu, Z. P. Lipid-encapsulated upconversion nanoparticle for near-infrared light-mediated carbon monoxide release for cancer gas therapy. *Eur. J. Pharm. Biopharm.* **2021**, *158*, 211−221.
(50) Opoku-Damoah, Y.; Zhang, R.; Ta, H. T.; Xu, Z. P. Vitamin E-facilitated carbon monoxide pro-drug nanomedicine for efficient light-responsive combination cancer therapy. *Biomater. Sci.* **2021**, *9* (18), 6086−6097.
(51) Dhara, K.; Lohar, S.; Patra, A.; Roy, P.; Saha, S. K.; Sadhukhan, G. C.; Chattopadhyay, P. A New Lysosome-Targetable Turn-On Fluorogenic Probe for Carbon Monoxide Imaging in Living Cells. *Anal. Chem.* **2018**, *90* (4), 2933−2938.
(52) Wu, M.; Zhang, Z.; Yong, J.; Schenk, P. M.; Tian, D.; Xu, Z. P.; Zhang, R. Determination and Imaging of Small Biomolecules and Ions Using Ruthenium(II) Complex-Based Chemosensors. In *Metal Ligand Chromophores for Bioassays*; Lo, K. K.-W., Leung, P. K.-K., Eds.; Springer International Publishing: Cham, 2023; pp 199−243.
(53) Liu, B.; Chen, Y.; Li, C.; He, F.; Hou, Z.; Huang, S.; Zhu, H.; Chen, X.; Lin, J. Poly(Acrylic Acid) Modification of Nd3+-Sensitized Upconversion Nanophosphors for Highly Efficient UCL Imaging and pH-Responsive Drug Delivery. *Adv. Funct. Mater.* **2015**, *25* (29), 4717−4729.
(54) Andresen, E.; Resch-Genger, U.; Schäferling, M. Surface Modifications for Photon-Upconversion-Based Energy-Transfer Nanoprobes. *Langmuir* **2019**, *35* (15), 5093−5113.
(55) Duong, H. T. T.; Chen, Y.; Tawfik, S. A.; Wen, S.; Parviz, M.; Shimoni, O.; Jin, D. Systematic investigation of functional ligands for colloidal stable upconversion nanoparticles. *RSC Adv.* **2018**, *8* (9), 4842−4849.
(56) Rolim, W. R.; Pieretti, J. C.; Renó, D. L. S.; Lima, B. A.; Nascimento, M. H. M.; Ambrosio, F. N.; Lombello, C. B.; Brocchi, M.; de Souza, A. C. S.; Seabra, A. B. Antimicrobial Activity and Cytotoxicity to Tumor Cells of Nitric Oxide Donor and Silver Nanoparticles Containing PVA/PEG Films for Topical Applications. *ACS Appl. Mater. Interfaces* **2019**, *11* (6), 6589−6604.
(57) Feng, C.; Xiong, Z.; Wang, C.; Xiao, W.; Xiao, H.; Xie, K.; Chen, K.; Liang, H.; Zhang, X.; Yang, H. Folic acid-modified Exosome-PH20 enhances the efficiency of therapy via modulation of the tumor microenvironment and directly inhibits tumor cell metastasis. *Bioact. Mater.* **2021**, *6* (4), 963−974.
(58) Kautz, A. C.; Kunz, P. C.; Janiak, C. CO-releasing molecule (CORM) conjugate systems. *Dalton Trans.* **2016**, *45* (45), 18045−18063.
(59) Singh, R. J.; Hogg, N.; Joseph, J.; Kalyanaraman, B. Mechanism of Nitric Oxide Release from S-Nitrosothiols. *J. Biol. Chem.* **1996**, *271* (31), 18596−18603.
(60) Zuckerbraun, B. S.; Chin, B. Y.; Bilban, M.; d'Avila, J. d. C.; Rao, J.; Billiar, T. R.; Otterbein, L. E. Carbon monoxide signals via inhibition of cytochrome c oxidase and generation of mitochondrial reactive oxygen species. *FASEB J.* **2007**, *21* (4), 1099−1106.

https://doi.org/10.1021/acsami.3c13165
ACS Appl. Mater. Interfaces 2023, 15, 56796−56806

Supporting Information

Simultaneous Light-Triggered Release of Nitric Oxide and Carbon Monoxide from A Lipid-Coated Upconversion Nanosystem Inhibits Colon Tumor Growth

Yaw Opoku-Damoah, Run Zhang, Hang T. Ta, and Zhi Ping Xu**

Y. Opoku-Damoah, R. Zhang, H. T. Ta, Z. P. Xu
Australian Institute for Bioengineering and Nanotechnology, The University of Queensland, Brisbane, QLD 4072, Australia
E-mail: gordonxu@uq.edu.au; r.zhang@uq.edu.au
H. T. Ta
School of Environment and Science, Griffith University, Brisbane, QLD 4111, Australia
H. T. Ta
Queensland Micro and Nanotechnology Centre, Griffith University, Brisbane, QLD 4111, Australia

Keywords: carbon monoxide, nitric oxide, light-triggered gas delivery, upconversion nanoparticle, colon cancer treatment

Supplementary Information includes:

1. Supplementary Figure S1-S10
2. Supplementary Table S1-S4
3. Supplementary Experimental Section

1. Supplementary Figure

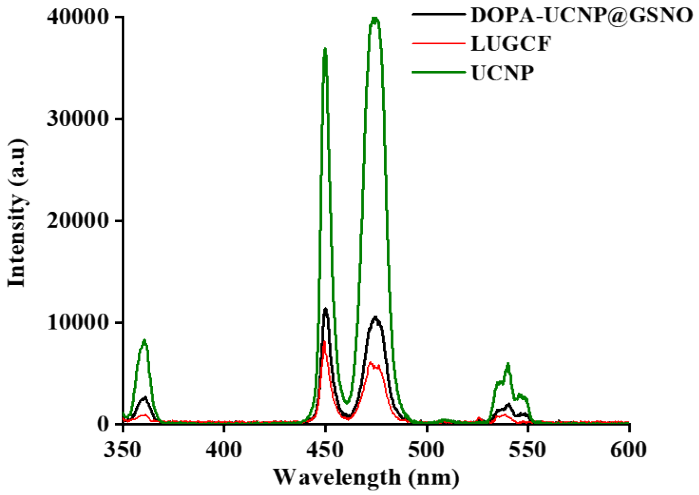

Figure S1. Photoluminescence spectra (980 nm, 1 W/cm^2) of UCNPs (5 mg), DOPA-UCNP@GSNO intermediary compound dispersed in cyclohexane and final LUGCF formulation in HEPES buffer.

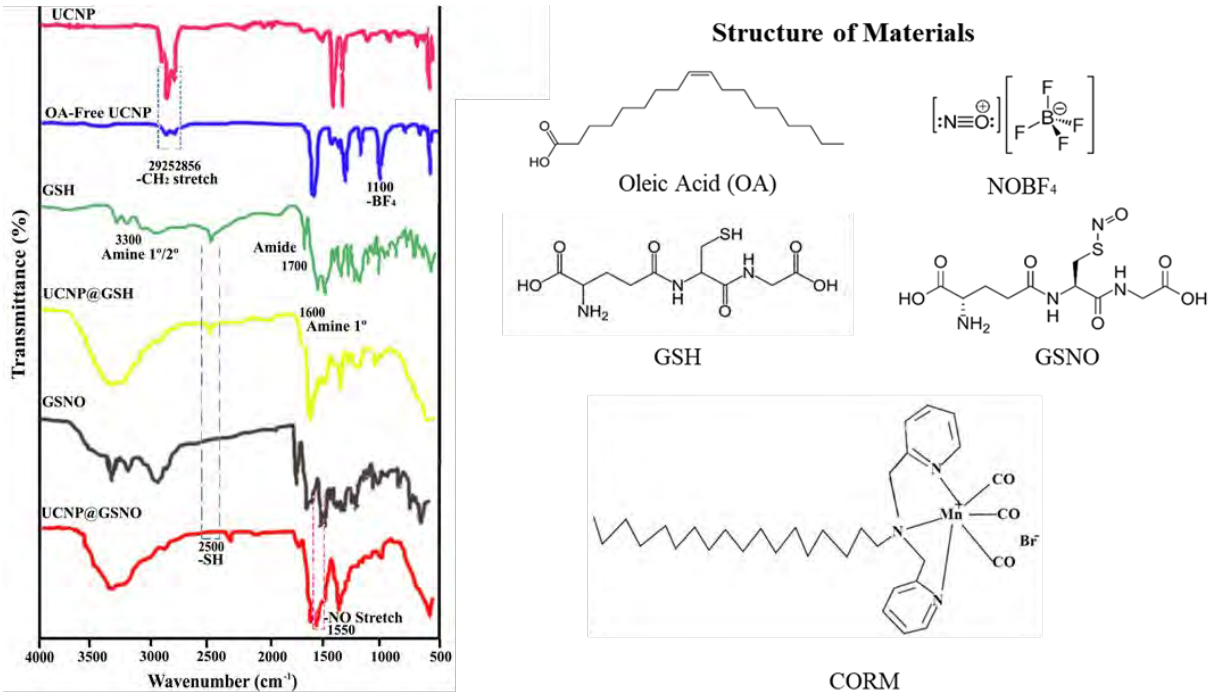

Figure S2. FTIR spectra of various formulations showing the starting materials during the step-wise nanosynthesis process to achieve the final LUGCF nanoformulation

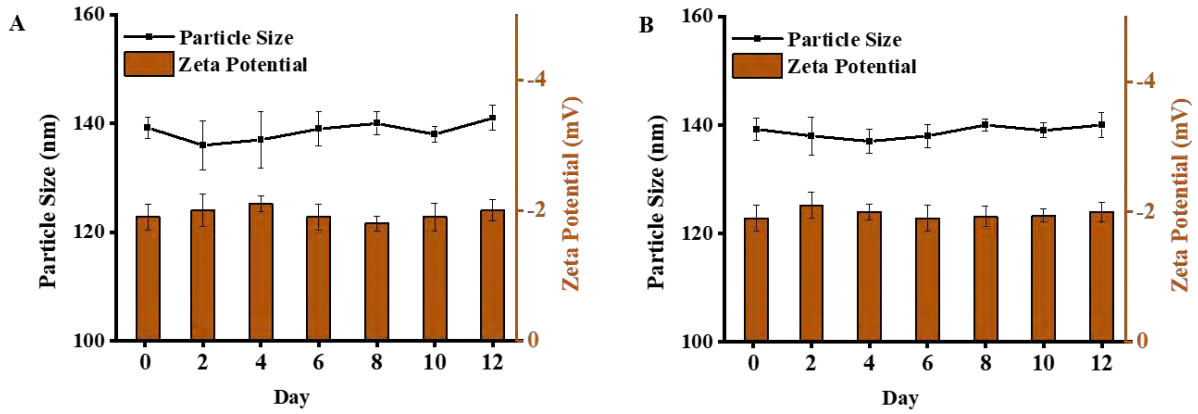

Figure S3. Characterization of nanoformulations with dynamic light scattering indicating the colloidal stability of LUGCF in (**A**) HEPES buffer (pH = 7.4) and (**B**) Cell culture medium (DMEM and 10 % FBS) for 12 days.

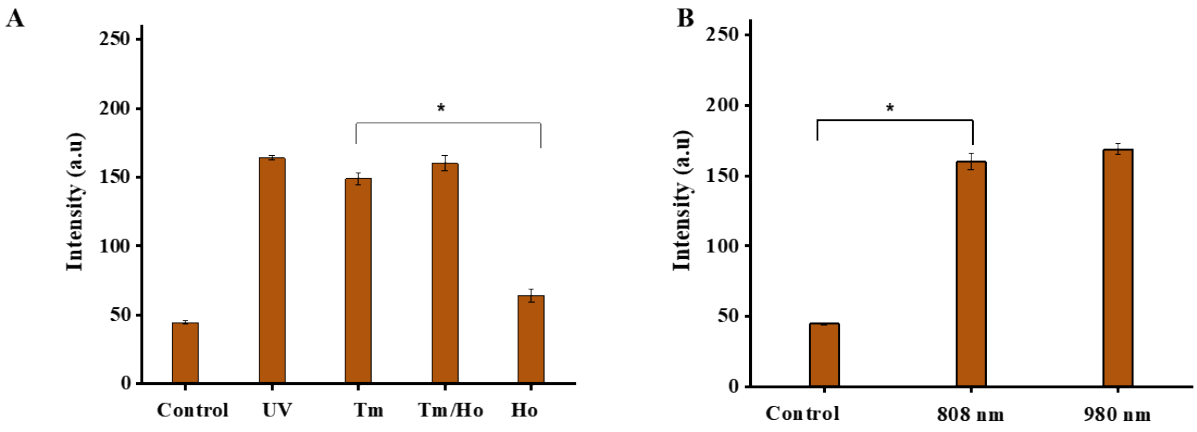

Figure S4. (**A**) Spectroscopic data for NO release with NIR lights using different UCNP core shell materials and UV light as secondary control group. NIR irradiation was performed at 808 nm 0.5 W/cm² in 5 min. Detection was performed 10 min after irradiation (λ_{ex} = 450 nm, λ_{em} = 600 nm). (**B**) Release of NO with different NIR lights using UCNP-NaYF4;Yb,Tm, Ho@NaYF4;Yb,Nd. NIR irradiation was performed at 980/808 nm 0.5 W/cm² in 5 min.

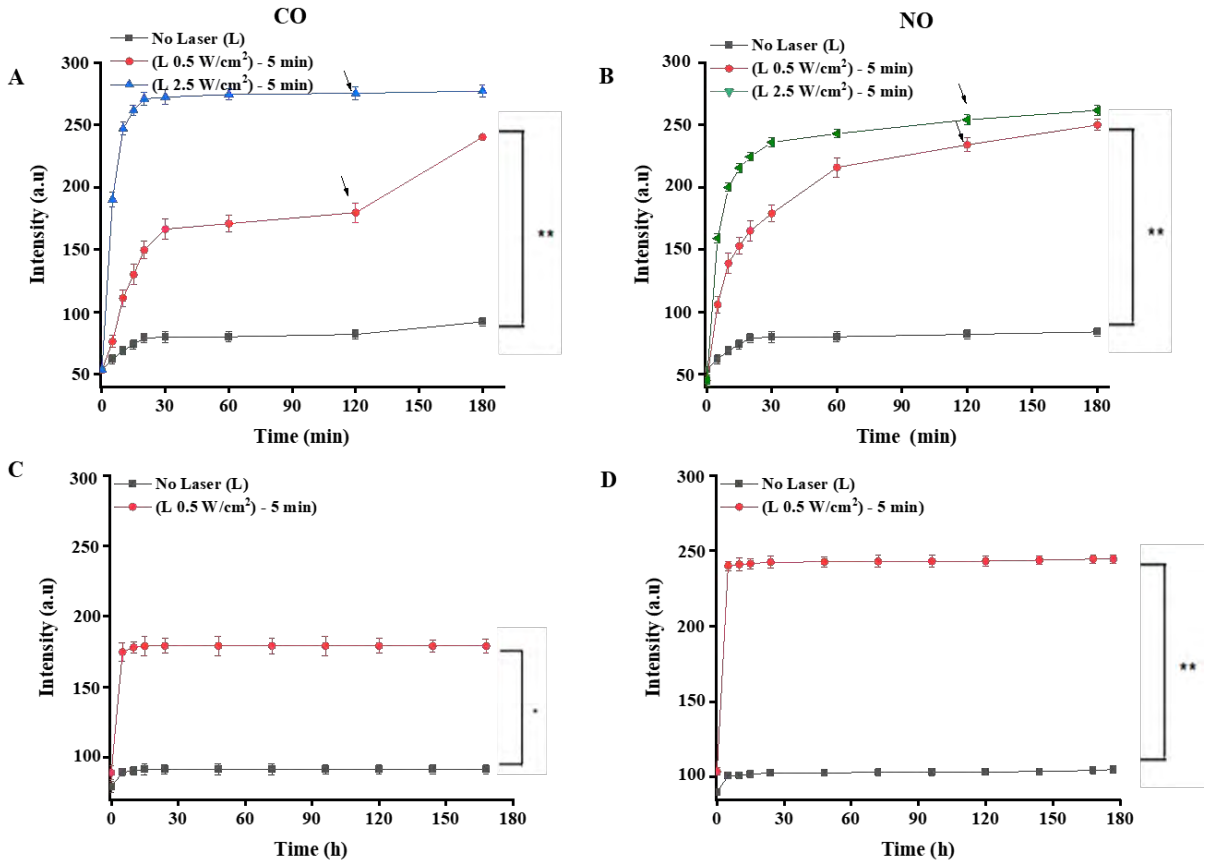

Figure S5. (**A**) Profile of CO release from LUGCF nanoformulation with 2nd irradiation after 2 h of observation detected by fluorescence spectroscopy of COFP at λ_{ex} = 450 nm, λ_{em} = 530 nm. (**B**) NO release from LUGCF nanoformulation with 2nd irradiation after 2 h of observation detected by NO fluorescent probe at λ_{ex} = 450, λ_{em} = 600 nm. (**C**) Long term/intraday CO release profile after first irradiation of LUGCF. (**D**) Long term/intraday NO release profile after irradiation of LUGCF. Light irradiations performed at 0.5 or 2.5 W/cm^2 for 5 min. Arrow indicates second irradiation point.

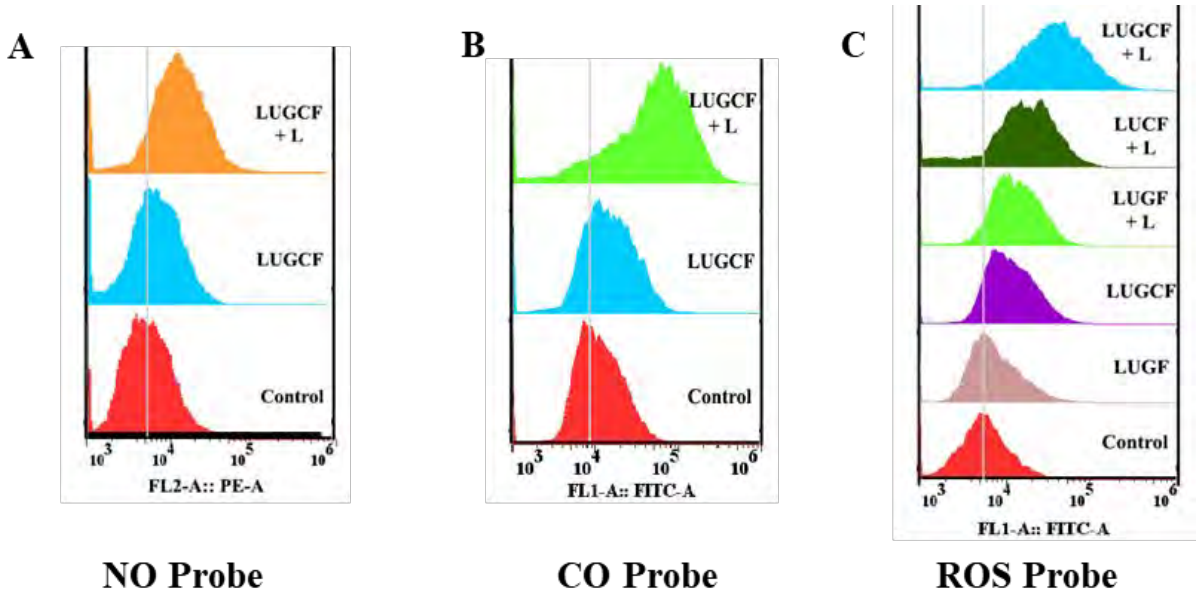

Figure S6. Flow cytometry data of HCT116 cells indicating the quantitative determination of (**A**) intracellular NO (**B**) cellular CO contents (**C**) ROS contents. Detection at λ_{ex} = 488 nm laser line and λ_{em} = 525 for ROS Probe (DCFH-DA)/ COFP and for NO probe λ_{em} = 600 nm. Nanoparticles replaced with fresh media after 4 h and irradiation groups (+L) treated with 808 nm light at 0.5 W/cm^2 for 5 min before further incubation and detection.

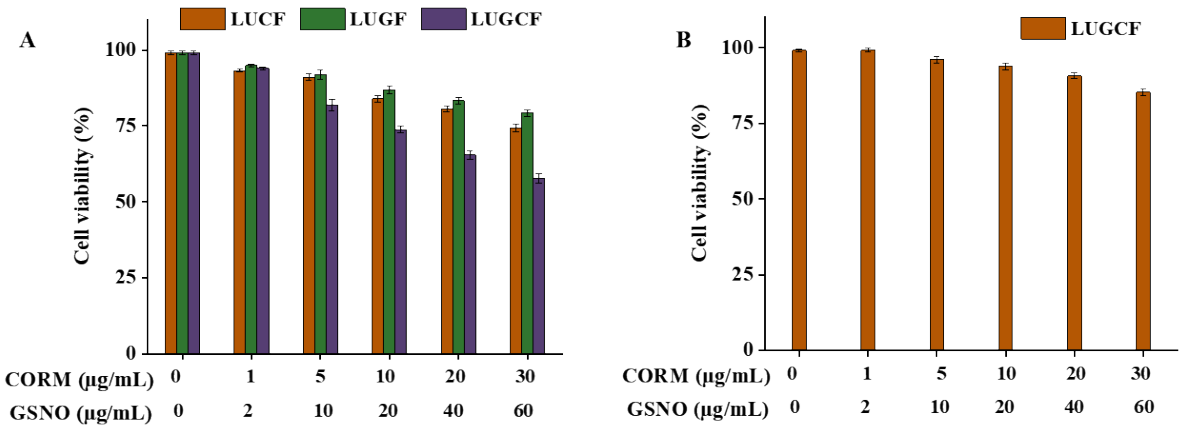

Figure S7. (A) MTT Assay for LUCF, LUGF and LUGCF nanoformulation (1:2 ratio) at various concentrations in HCT116 cells without laser (L) irradiation **(B)** Cell viability assay of LUGCF without laser (L) irradiation in HEK293T cells. All nanoparticles in A were replaced with fresh media after 4 h, and that in B were maintained. Incubation for a total of 48 h was observed before MTT assessment**.**

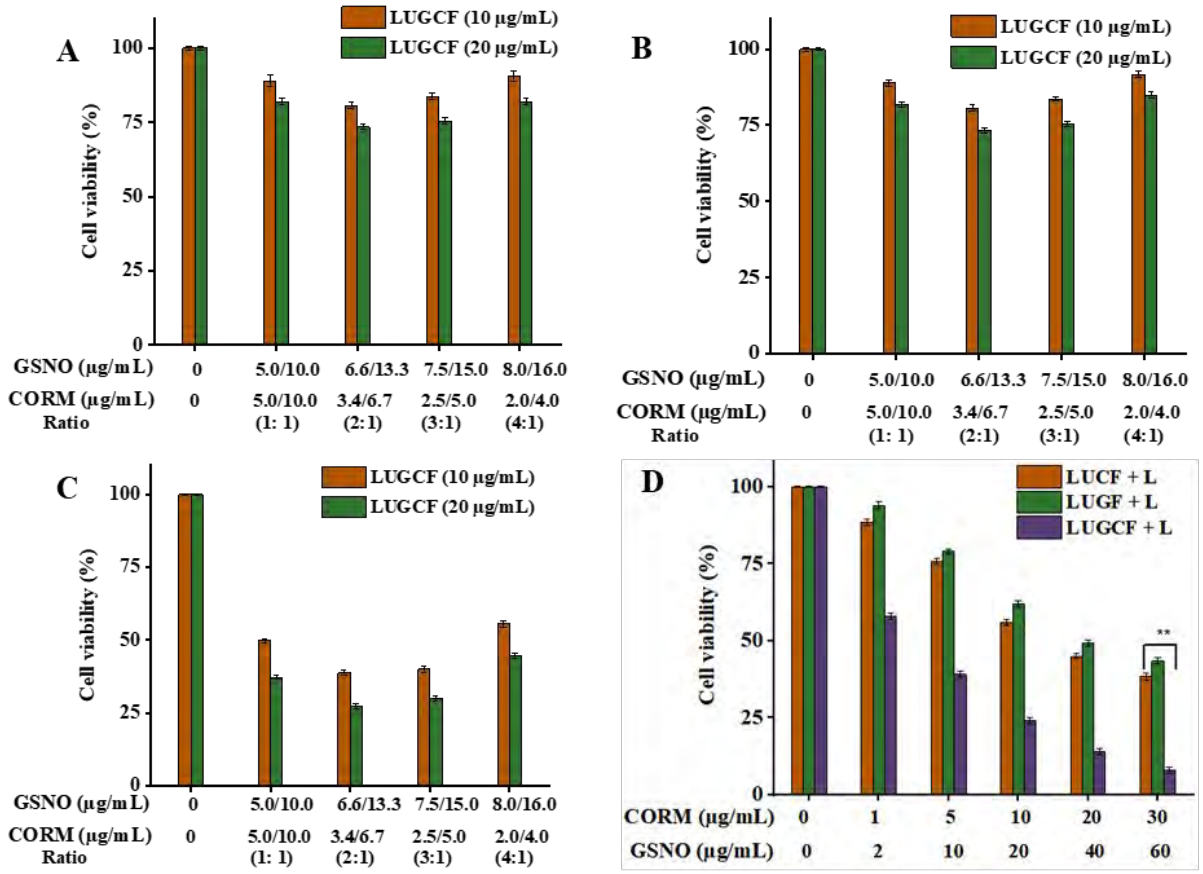

Figure S8. MTT Assay for different ratios and combinations of LUGCF nanoformulation at 10 and 20 μg/mL in (**A**) HCT116 cells without light irradiation, (**B**) CT26 cells without light irradiation, (**C**) CT26 cells with laser irradiation. (**D**) Cell viability assay of various concentrations of nanoformulations in CT26 cells. All nanoparticles were replaced with fresh media after 4 h and irradiation groups (+L) treated with 808 nm light at 0.5 W/cm^2 for 5 min, followed by incubation for a total of 48 h before MTT assay.

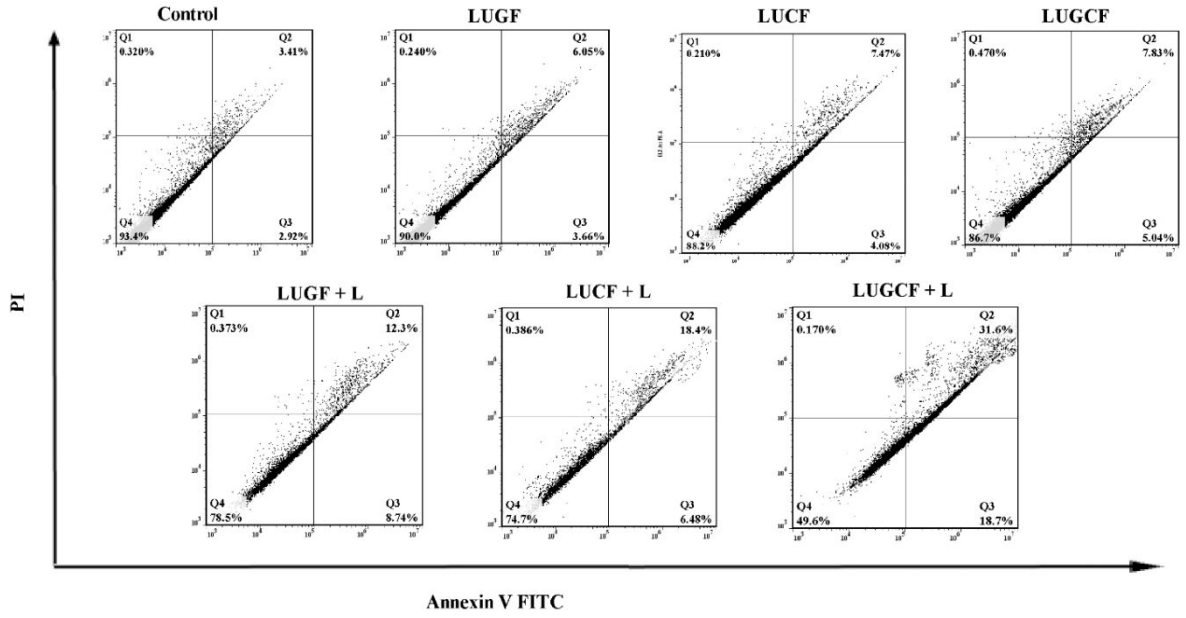

Figure S9. Cell apoptosis assay of various formulations (3.4/1.7 μg/mL of GSNO/CORM concentration) showing the apoptotic and necrotic profiles of HCT116 cells after 24 h of incubation. All nanoparticles were replaced with fresh media after 4 h and irradiation groups (+L) treated with 808 nm light at 0.5 W/cm^2 for 5 min, followed by incubation for a total of 24 h before PI-Annexin V FITC staining and analysis.

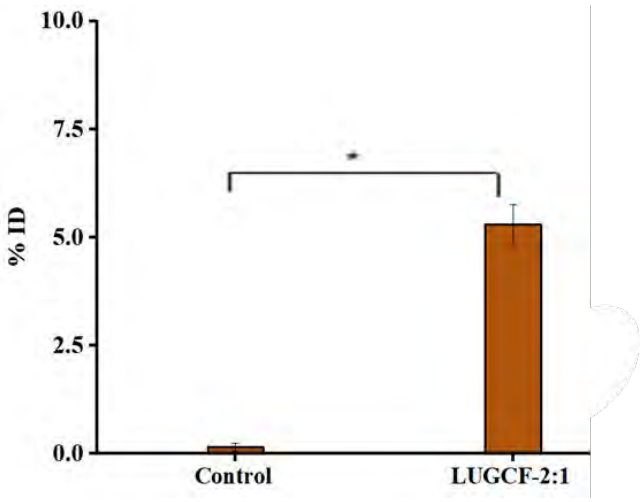

Figure S10. Elemental analysis of Mn contents in excised tumours after 24 h of administration. 0.2 g of tumours were analysed per tumour sample and 5.3% of CORM accumulated in tumours.

2. Supplementary Table

Table S1. Elemental analysis contents of GSNO after synthesis. The successful formation of GSNO was confirmed by CHNS/O elemental analysis, in which an overall weight yield of 84.3% and an average of 99.7% nitrogen and carbon purity were detected after recovery of the powdered sample.

Sample	N	C	H	S
GSNO (Theoretical)	16.65	35.68	4.76	9.51
GSNO	16.62	35.65	4.73	8.29

Table S2. IC_{50} values for various nanoformulations after 48 h of treatment.

Formulation	IC50 (µg/mL)/µM GSNO	IC50 (µg/mL)/µM CORM	IC50 (µg/mL)/µM GSNO
LUCF	-	198.1	-
LUGF	211.3	-	211.3
LUCF + L	-	12.9/8.7	-
LUGF + L	41.6	-	41.6
LUGCF	93.0	46.5	93.0
LUGCF + L	3.4	1.7	3.4

Table S3. MTT summary for combination therapy and corresponding LUGF/LUCF (with laser treatment). Cell viabilities extrapolated from tested groups after light irradiation.

CORM/GSNO mass ratio	CORM/GSNO (dose, µg/mL)	LUCF Viability	LUGF Viability	LUGCF Viability	Combination index	Average Combination index
1:1	5/5	73.5	87.9	49.7	1.29	1.26
	10/10	57.0	79.9	37.2	1.23	
2:1	3.4/6.7	80.5	85.0	38.7	1.77	1.85
	6.6/13.3	67.4	77.5	27.1	1.93	
3:1	2.5/7.5	84.7	83.6	39.3	1.80	1.84
	5,15	73.5	75.0	29.5	1.87	
4:1	2,8	87.2	83.0	54.2	1.34	1.34
	4,16	77.6	74.1	43.0	1.34	

Coefficient of drug interaction= Survival ratio (LUCF)× Survival %(LUGF)

Survival ratio (LUGCF)

Average CI = $\sum$ CI / number of dosages

A*B/C ratio:<0.8:asynergy, 0.8-1.2:additive, 1.2-1.4:mild synergy, 1.4-1.6:moderate synergy, >1.6:strong synergy

Table S4. MTT summary for combination therapy and corresponding LUGF/LUCF (without laser treatment). Cell viabilities extrapolated from tested groups.

CORM/GSNO mass ratio	CORM/GSNO (dose, µg/mL)	LUCF Viability	LUGF Viability	LUGCF Viability	Combination index	Average Combination index
1:1	5/5	86.4	95.4	86.8	0.95	0.94
	10/10	78.6	91.7	77.8	0.93	
2:1	3.4/6.7	89.7	94.0	80.7	1.01	1.02
	6.6/13.3	83.5	89.7	73.4	1.02	
3:1	2.5/7.5	91.7	93.4	83.7	1.02	1.02
	5,15	86.4	88.9	75.4	1.02	
4:1	2,8	92.9	93.0	90.6	0.95	0.95
	4,16	88.4	88.4	81.9	0.95	

3. Supplementary Experimental Section

Materials

Sodium hydroxide (NaOH) was obtained from Chem-Supply. Cholesterol, 1,2-dioleoyl-sn-glycero-3-phosphocholine (DOPC), 1,2-dioleoyl-sn-glycero-3-phosphate (DOPA), 1,2-distearoyl-sn-glycero-3-phosphoethanolamine-N-(polyethylene glycol)-2000 (DSPE-PEG) and 1,2-dioleoyl-sn-glycero-3-phosphoethanolamine-N-(lissamine rhodamine B sulfonyl) (18:1 Liss Rhod PE), and 1,2-distearoyl-sn-glycero-3-phosphoethanolamine-N-[folate (polyethyleneglycol)-2000 (DSPE-PEG-FA) were obtained from Avanti Polar Lipids, USA. Lanthanides chloride hexahydrate ($TmCl_3 \cdot 6H_2O$, $NdCl_3 \cdot 6H_2O$, $YCl_3 \cdot 6H_2O$, $YbCl_3 \cdot 6H_2O$), ammonium fluoride (NH_4F), oleic acid (99% purity), sodium nitrite ($NaNO_2$), Nitrosyl tetrafluoroborate ($NOBF_4$), oleylamine (OM), and 1-octadecene (ODE) were obtained from Merck KgaA (Darmstadt, Germany). Dulbecco's Modified Eagle Medium (DMEM) and fetal bovine serum (FBS) were purchased from Gibco, USA. DCFH-DA ROS assay kit was purchased from Promokine. Annexin V-FITC cell apoptosis detection kit and JC-1 mitochondria assay kit were purchased from Invitrogen (by Thermofisher Scientific). All other chemicals used were obtained from Merck KgaA (Darmstadt, Germany) and were of HPLC or analytical grade.

Synthesis of core-shell upconversion nanoparticles (UCNPs)

Core UCNPs ($NaYF_4$:Yb,Ho,Tm) were first synthesized using the thermal decomposition method. Under nitrogen gas atmosphere, $YCl_3.6H_2O$ (0.785 mmol), YbCl3.6H2O (0.2 mmol), $HoCl_3.6H_2O$ (0.001 mmol) and $TmCl_3.6H_2O$ (0.005 mmol) in a three-neck round bottom flask were dissolved with 6 mL of oleic acid (OA) and 15 mL of 1-octadecene (ODE) at 150 ºC for 60 min. Upon cooling to room temperature, 10 mL of methanol solution containing 0.148 g of ammonium fluoride (NH_4F) and 0.1 g of sodium hydroxide (NaOH) was added. The mixture was stirred for another 60 min at room temperature, and then slowly heated to 120 ºC for 30 min to get rid of methanol. The temperature was then rapidly increased to 310 ºC for 90 min.

After cooling down to room temperature, 10 mL of ethanol was added to precipitate the UCNPs. The formed UCNPs were then washed with methanol, ethanol, and cyclohexane three times. The synthesized UCNPs were dispersed in 10 mL of cyclohexane and stored at 4 ºC for subsequent use.

The shell nanocrystal seeds (α-$NaYF_4$:Nd) (2 mmol) were prepared with the same thermal decomposition procedure. Typically, $YCl_3.6H_2O$ (1.4 mmol) and $NdCl_3.6H_2O$ (0.6 mmol) were magnetically dissolved in 12 mL of OA, 6 mL of oleylamine (OM) and 20 mL of ODE at 150 ºC for 60 min. After cooling down to room temperature, methanol solution (10 mL) containing 0.296 g NH_4F and 0.2 g NaOH was added, and the slurry was stirred at room temperature for another 30 min. Then, the reaction mixture was heated to 120 ºC for 30 min to remove methanol, followed by heating to 290 ºC for 30 min to produce α-$NaYF_4$:Nd. The resultant α-$NaYF_4$:Nd seeds obtained were dispersed in cyclohexane (2.0 mmol in 10 mL).

The core-shell nanoparticles ($NaYF_4$:Yb,Ho,Tm@$NaYF_4$:Nd) were synthesized by coating $NaYF_4$:Yb,Tm cores with α-NaYF4:Nd nanocrystal seeds as follows: $NaYF_4$:Yb,Tm (2 mL/0.2 mmol) cores stocked in cyclohexane were magnetically mixed with OM (1 mL), OA (5 mL) and ODE (8 mL). α-$NaYF_4$:Nd shells to be used for the coating were processed by replacing cyclohexane with 1.5 mL of OM, 7 ml of OA and 11.5 mL of ODE by heating to 110 ºC for 30 min under nitrogen gas. Upon heating the core nanoparticles to 303 ºC, the $NaYF_4$:Yb,Ho,Tm core was quickly injected with 0.3 mL of α-NaYF4:Nd nanocrystal seeds using a syringe, followed by the addition of 0.2 mL every 10 min until the desired core: shell mass ratio (1:0.25, 1:0.5, 1:0.75 or 1:1) was achieved. After the last injection, the mixture was kept at 303 °C for 30 min to obtain the final core-shell $NaYF_4$:Yb,Ho,Tm@$NaYF_4$:Nd UCNPs. The precipitate was collected, washed and re-dispersed in cyclohexane using the same procedure for synthesizing core UCNPs.

Synthesis of Gas Releasing Molecules

$C_{30}H_{49}N_3Mn(CO)_3Br$ CORM was synthesized according to the method described previously by Sakla et al [1]. GSNO was also synthesized according to the method described by Hart et al. with a slight modification [2]. The NO molecule was prepared by adding 5mM of sodium nitrite ($NaNO_2$) to an equimolar amount (8.1 mmol) of glutathione (GSH) in 8 mL of deionized water containing HCl (2.5mL). The red mixture was stirred continuously for 40 min at 4 ºC before neutralization with acetone (10 mL) for 10 min. The final fine pale solid was centrifuged at 2000 × g for 3 min and washed with excess ice-cold water, acetone and ether to produce a pale red solid which was kept in a desiccator to dry.

Synthesis of DOPA-UCNP@GSNO

Core-shell UCNPs were initially prepared by thermal decomposition method described previously with a little modification to accommodate Holmium (Ho) [3]. The surface of $NaYF_4$,Yb,Ho,Tm@NaYF4;Nd UCNPs were modified with hydrophilic GSNO by the ligand exchange method described by Chen et al [4]. Oleic acid (OA) UCNP capping was removed by the addition of 5 mL of $NOBF_4$ (0.1 M) in N,N-dimethylformamide (DMF) to 5 mL of UCNPs dispersed in cyclohexane (10 mg/mL). The mixture was shaken vigorously for 10 min and allowed to stand to separate the mixture into two visible layers of solvent. The upper layer containing cyclohexane was removed, while the bottom layer containing UCNPs were purified with excess amount of hexane and toluene (1:1 v/v). The mixture was then centrifuged at 3500 x g for 10 min, washed and subsequently redispersed in DMF. UCNPs (5 mg) was incubated with 1 mg of GSNO for 8 h, followed by 0.57 µmol of lipid (1, 2-dioleoyl-sn-glycero-3-phosphate-DOPA) for another 8 h. The mixture was centrifuged at 7000 x g for 10 m and the pellet was dispersed in chloroform to obtain amphiphilic DOPA-UCNP@GSNO. Different ratios of UCNP and GSNO for optimization were prepared by the same procedure with variable amounts (0.5, 1.0, 1.5 and 2.0 mg) of GSNO.

Cell Culture

Human colorectal carcinoma cell lines (HCT116) and murine colorectal carcinoma cell line (CT26) were grown in 90% DMEM supplemented with 10% FBS 100 U/mL penicillin, and 100 mg/mL streptomycin. Exponentially growing cultures were maintained in a humidified chamber containing 5% CO_2 at 37 ℃ throughout the cell studies.

Cell viability assay

CT26 and HCT116 cells at the density of 1×10^4 cells/well were seeded in 96-well plates with 100 µL of culture medium. After 24 h incubation, cell culture media in all groups were replaced with FBS-free media containing gaseous drugs (0-30 and 0-60 µg/mL of CORM and GSNO, respectively). MTT assay was used to measure the cell viability of CT26 cells after incubation with LUGF, LUGF + L, LUCF, LUCF + L, LUGCF-2:1 and LUGCF + L-2:1, where L represents 808 nm laser irradiation (0.5 W/cm^2, 5 min). After 4 h, the culture media were discarded and replaced with fresh media, followed by the NIR light (808 nm, 0.5 W/cm^2) irradiation for another 5 min (+ L). Both laser-irradiated and no irradiation groups were subsequently incubated for another 48 h before the addition of 10 µL MTT solution (5 mg/mL) to respective wells. Media was replaced with 100 µL of DMSO after 4 h to dissolve the staining chemical in each well. Cell viability assay was employed to compare the effectiveness of the amounts of both CO and NO gases. Firstly, different combinations of GSNO:CORM (1:1, 2:1, 3:1, and 4:1) were used to determine the most effective combination *via* MTT cell viability assay. The same process was applied to all MTT experiments using these combinations of CORM and GSNO. The absorbance was finally measured at 570 nm (absorbance at 670 nm as the reference) using Tecan Infinite M200 PRO Multimode Microplate Reader (Switzerland). The cell viability was expressed as a percentage of the untreated control cells, as reported previously.

Statistical analysis

All data are presented as mean ± standard error of the mean (SEM) from at least triplicate experiments conducted in a parallel manner, unless otherwise stated. The differences among

various groups were analyzed using one-way analysis of variance (ANOVA), and the significance was indicated as *: $p < 0.05$, **: $p < 0.01$, and ***: $p < 0.001$.

References

[1] R. Sakla, D.A. Jose, Vesicles Functionalized with a CO-Releasing Molecule for Light-Induced CO Delivery, ACS Appl Mater Interfaces, 10 (2018) 14214-14220.

[2] T.W. Hart, Some observations concerning the S-nitroso and S-phenylsulphonyl derivatives of L-cysteine and glutathione, Tetrahedron Letters, 26 (1985) 2013-2016.

[3] Y. Opoku-Damoah, R. Zhang, H.T. Ta, D. Amilan Jose, R. Sakla, Z. Ping Xu, Lipid-encapsulated upconversion nanoparticle for near-infrared light-mediated carbon monoxide release for cancer gas therapy, Eur J Pharm Biopharm, (2020).

[4] G. Chen, J. Damasco, H. Qiu, W. Shao, T.Y. Ohulchanskyy, R.R. Valiev, X. Wu, G. Han, Y. Wang, C. Yang, H. Ågren, P.N. Prasad, Energy-Cascaded Upconversion in an Organic Dye-Sensitized Core/Shell Fluoride Nanocrystal, Nano Letters, 15 (2015) 7400-7407.